SNPO-C
Reilly

RECORD COPY

NUCLEAR ROCKET OPERATIONS

SACRAMENTO PLANT

REPORT NO. RN-S-0424A

TO

AEC-NASA SPACE NUCLEAR PROPULSION OFFICE

UNCERTAINTY ANALYSES FOR RADIATION EFFECTS TESTS

NERVA PROGRAM CONTRACT SNP-1

NOVEMBER 1967

ADDENDUM

TO

RN-S-0424

MASTER

NUCLEAR PRODUCTS AND SERVICES GROUP

AEROJET GENERAL TIRE GENERAL

AEROJET-GENERAL CORPORATION

SACRAMENTO, CALIFORNIA

DISCLAIMER

AEROJET GENERAL TIRE GENERAL

REPORT NO. RN-S-0424A

UNCERTAINTY ANALYSES FOR RADIATION EFFECTS TESTS

NOTICE

PORTIONS OF THIS REPORT ARE ILLEGIBLE. IT [illegible] from the best available copy to permit the broadest possible availability.

NERVA PROGRAM CONTRACT SNP-1

NUCLEAR ROCKET OPERATIONS

NOVEMBER 1967

CLASSIFICATION CATEGORY

UNCLASSIFIED

R A Greenhow 11-1-67

CLASSIFYING OFFICER DATE

AEROJET-GENERAL CORPORATION
A SUBSIDIARY OF THE GENERAL TIRE & RUBBER COMPANY

DISTRIBUTION OF THIS [illegible]

50

REPORT NO. RN-S-0424A

UNCERTAINTY ANALYSES FOR RADIATION EFFECTS TESTS

R. H. Sanders
E. A. Thomas

C. M. Rice
Program Manager
Nuclear Rocket Operations

FOREWORD

Aerojet-General report RN-S-0424 was written to define the uncertainty involved in the thermal conductivity experiments to be conducted at General Dynamics, Fort Worth.

Since its publication in August 1967, the analyses have been refined to consider several sources of measurement uncertainty which proved to be of lesser magnitude than originally believed. Also, a more detailed and rigorous thermal analysis of steady-state and transient heat leaks has been made for the apparatus. Both of these refined analyses are documented in this addendum.

The addendum is divided into two parts. The first part describes the modifications made to the measurement uncertainty analysis while the second defines the refinements to the thermal analysis.

A number of replacement pages to RN-S-0424 also are supplied with this addendum. These pages document the modifications to the measurement uncertainty analysis. They were prepared as an integral part of the refined analysis; however, they have been separated from this addendum to facilitate their insertion into the original analysis, Report RN-S-0424.

CONCLUSIONS

The following instrumentation and thermal analysis modifications to the Uncertainty Analysis for Radiation Effects, Aerojet-General report RN-S-0424, reflect an improved overall test uncertainty for the thermal conductivity experiment. Through these modifications, the overall measurement uncertainty in the thermal conductivity experiment approaches a value less than 1%; however, systematic uncertainties and heat losses reduce the overall experimental accuracy slightly. The refined thermal analyses have been used to estimate the following heat losses at a $\Delta T = 220°K$ using liquid nitrogen as a cryogenic reference bath.

	Maximum Heat Loss (%) at $\Delta T = 220°K$		
Material	Original Analysis	Refined Analysis	Change [%]
P-03	18.0	6.5	- 11.5
Be	.45	1.75	+ 1.3
Al	1.0	2.2	+ 1.2
Ti	5.5	13.0	+ 7.5

A thermal analysis also was conducted to define the heat losses occurring using Freon 114 as a secondary cryogenic reference bath. Figures 9 through 11 of the refined thermal analysis indicate a heat loss of approximately 10% at a ΔT of 350°K corresponding to an absolute temperature of approximately 760°K at thermocouple TC_3 using the Freon 114 bath. This temperature should be considered the maximum attainable for data within $\pm$ 10% accuracy. However, data acquisition will be limited to a ΔT of 220°K using Freon 114 due to power limitations of the heaters.

UNCERTAINTY ANALYSIS
FOR
REPORT NO. RN-S-0424
MODIFICATION A
OF TEXT

INSTRUMENTATION
MODIFICATION TO UNCERTAINTY ANALYSIS FOR
RADIATION EFFECTS TESTS

R. H. Sanders

INSTRUMENTATION
MODIFICATION TO UNCERTAINTY ANALYSIS FOR
RADIATION EFFECTS TESTS

This section of the addendum describes modifications made to the text of Aerojet-General report RN-S-0424, Uncertainty Analysis for Radiation Effects Tests. Essentially these modifications reflect a reduced data acquisition uncertainty for temperature-measurement signals.

The discussion that follows describes the basis for the modifications. The actual changes have been incorporated into replacement pages 3, 6, 29, 30, 31, 33 and 34 to report RN-S-0424. These pages are an integral part of the modified uncertainty analysis but are not bound as a part of this document to facilitate their insertion into the basic report.

The original analysis was based upon the random selection of thermocouple wire from various spools and the non-selective fabrication of thermocouple junction and splices. In reality, all wire splices of similar thermocouple materials for the actual thermal conductivity test apparatus were made using wire from a single calibrated spool. This procedure greatly decreases the inherent uncertainty of each temperature recording channel. The replacement pages reflect this revised procedure with its attendant reduction in uncertainty.

Figure 2 of report RN-S-0424 illustrates two splices of dissimilar materials that are present at the copper tempering ring in each thermocouple channel. Splices such as these potentially can produce erroneous emf's if appreciable temperature gradients exist at the tempering ring. A slight temperature drift occurs at these splices on the tempering ring when the cryogenic bath is liquid nitrogen. This temperature drift is shown in Figures C-6, C-7, and C-8 of Appendix C to report RN-S-0424. These splices potentially produce larger emf's when Freon 114 is used as a secondary cryogenic reference bath due to the presence of the temperature gradients defined in revised Figures 19 - 22 of Addendum to Appendix C of the report.

Measurements of the emf's generated without power applied to the test apparatus were made to define the total uncertainty for each recording circuit. The apparatus was in thermal equilibrium at both liquid nitrogen and room temperatures when these measurements were made. This procedure will

be repeated during the post-irradiation and post-annealing cycle to determine if any nuclear-induced changes occur in the emf's generated without power to the apparatus and to define the upper limit of the erroneous emf's produced by the temperature drift of the copper tempering rings. This calibration procedure will also be repeated for the Freon 114 bath. Pre-irradiation measurements of generated emf's for each thermocouple channel indicated that a maximum emf of $\pm$ 5 uv was induced in the apparatus at both room or liquid nitrogen temperatures.

Post-test zero-potential calibration should prove that the extraneous emf's produced by the dissimilar metal junction on the tempering ring are negligible.

Through the use of calibrated thermocouple materials and reference bath calibration corrections, the total thermocouple uncertainty equation reduced to:

$$\text{Measurement uncertainty*} = \left[\left(\pm \begin{matrix}\text{wire} \\ \text{calibration} \\ \text{uncertainty}\end{matrix} \right)^2 + \left(\begin{matrix}\text{transition} \\ \text{uncertainty}\end{matrix} \right)^2 + \left(\begin{matrix}\text{meter} \\ \text{uncertainty}\end{matrix} \right)^2 \right]^{\frac{1}{2}}$$

In microvolts, the measurement uncertainty is:

$$\text{RSS} = \left[(3)^2 + (5)^2 + (5)^2 \right]^{\frac{1}{2}}$$

$$\text{RSS} = \pm 7.7 \text{ uv/channel}$$

The uncertainty in temperature versus microvolts corresponding to this RSS value is presented in Table IV and Figure 3. The replacement pages attached to this document reflect this reduced uncertainty.

*Refer to report RN-S-0424 for detailed discussion of measurement uncertainty.

UNCERTAINTY ANALYSIS
FOR
REPORT NO. RN-S-0424
ADDENDUM TO
APPENDIX C

ADDITIONAL ANALYTICAL THERMAL ANALYSIS
FOR RADIATION EFFECTS TEST 37/R 104
(THERMAL CONDUCTIVITY)

E. A. Thomas

TABLE OF CONTENTS

I. INTRODUCTION

This report is published as an addendum to Appendix C of Aerojet Report RN-S-0424.[1] It provides a more detailed and rigorous analysis of steady-state and transient heat leaks for the test apparatus. Freon 114 was considered as a secondary bath for this analysis to obtain more accurate data for P-03 graphite above room temperature. Curves of expected reference-ring temperature-rise versus specimen ΔT for the Freon 114 bath are included for all specimens. This report also contains the results of an analysis to determine the temperature measurement error caused by differences in temperature between the specimen and shield. Figures 5 through 11 of this report supersede Figures C-1 through C-5 of Report RN-S-0424.

II. SUMMARY

Steady-state and transient thermal leakage was estimated for beryllium, aluminum 7039, P-03 graphite, Inconel 718, and titanium 5AL-2.5 Sn III specimens.

The steady-state heat leakage was estimated using analytical models improved from the ones described in RN-S-0424. A similar model was used to estimate the leakage for aluminum and beryllium specimens. However, this model also included the effect of multiple reflections in the radiation interchange. Models for titanium and Inconel had double the number of nodes in addition to the effect of multiple reflections. Models for the graphite specimen had twice the original number of nodes with special emphasis on the effect of thermal leakage to the metal backing plate of the graphite shield. Analyses for graphite specimens also were made for shields of aluminum, stainless steel, as well as for a glass-fiber wrapper used in place of the shield.

---

[1] Uncertainty Analyses for Radiation Effects Tests, Aerojet-General Report RN-S-0424, August 1967.

The transient drift contribution to the overall leakage was upgraded by including the drift caused by the specimen itself.

The bias in thermocouple reference junction temperature resulting from heat flow into the test cell cap from the specimen and shield was computed assuming Freon 114 as a reference bath. Calculations were made for each specimen.

Temperature measurement errors caused by the thermocouple junction being located on the clamp, which results in measurement of temperatures different from the specimen temperatures also were computed. Source of this type of error is the dissimilar temperatures of the specimen and shield at corresponding locations. This error is a function of the relative thermal resistances in the circuit between the specimen and shield.

III. DISCUSSION

A. ANALYSIS OF STEADY-STATE HEAT LEAKS

1. Steady-State Analytical Models

The steady-state thermal leakage of the specimen was estimated by constructing an analytical model of the experimental apparatus. This was accomplished using a resistor network in conjunction with Computing Sciences Job E12901 programmed for the IBM 360/65 computer. Job E12901 is essentially the same program as Job 278[2] except that it is written for the IBM 360/65 computer rather than the IBM 7094 computer.

The network consists of one-dimensional conduction resistors in the specimen rod and shield shell (for all models except for the graphite

[2] Thermal Network Analyzer, Aerojet-General Computing Sciences Job 278, August 1962.

composite shield), a two-dimensional conduction network in the heater core and copper heat sink, conduction resistors between specimen and shield representing tempering and resistivity leads, convection resistors between the heat sink and reference bath, and radiation resistors interconnecting the specimen, shield, and sink. The analytical models used in this analysis are more detailed than those used in the original analysis contained in Reference 1. In all cases, except the graphite specimen which uses a composite of graphite, mica and steel, the shield is assumed to be of the same material as the specimen.

Steady-state analyses at various temperature differentials across the specimen were made by heating the surface of the heater uniformly to simulate the heater windings and allowing the temperature distribution in the network to reach equilibrium. Analyses were made for specimen ΔT values ranging from 60 to 220°K for the metallic specimens and from 60 to 350°K for graphite specimens. The heat sink was exposed to boiling liquid nitrogen for all models. Boiling Freon 114 also was considered as an additional reference bath for the graphite specimen to obtain data at a higher absolute temperature without imposing extremely high ΔT values on the specimen which would result in high losses due to thermal radiation. Pool-boiling film coefficients for the liquid nitrogen bath were obtained from NBS Technical Note 317.[3] Similar coefficients for Freon 114 also were obtained.[4] Thermal conductivity characteristics for aluminum 7039, unirradiated P-03 graphite, titanium 5 Al 2.5 Sn-ELI and Inconel 718 were obtained from Aerojet-Materials Properties Data Book.[5] Conductivity data for commercial grade beryllium were obtained from

---

[3] Boiling Heat Transfer for Oxygen, Nitrogen, Hydrogen, and Helium, NBS Technical Note 317, 20 September 1965.

[4] ASHRAE Handbook of Fundamentals, Chapter 3, P. 47, Figure 10.

[5] Materials Properties Data Book, Aerojet-General Report 2275, Revised 15 March 1967.

the data of Powell, Hardin and Gibson[6]. Conductivity trends for AWG graphite were obtained from Figure 3 of North American Aviation Report NAA-SR-862[7] and used for estimating the thermal conductivity of irradiated P-03 graphite.

Features of the thermal models used for the various specimens are described in the following paragraphs.

2. Beryllium and Aluminum Models

The coarse network shown in Figure 1 was used for analysis of beryllium and aluminum specimens. This network is similar to that used in the original analysis described in the Report RN-S-0424 except for the radiation resistors. These resistors were added to simulate the energy reflected to the specimen rod and cylindrical shield as well as direct radiation reflected from the shield back to itself. Grey-body shape-factors were computed for all radiation resistors assuming that all direct and reflected radiation was diffuse. An emissivity value of 0.1, as recommended by Touloukian[8], was used in the computation of grey-body shape-factors for both the beryllium and aluminum models.

3. Inconel and Titanium Models

The fine network shown in Figure 2 was used for analysis of Inconel and titanium specimens. This network differs from the coarse network in that it has twice as many resistors in the specimen and shield portions.

---

[6] Powell, R. L., Hardin, J. L., and Gibson, E. F., "Low-Temperature-Transport Properties of Commercial Metals and Alloys, IV. Reactor Grade Be, Mo and W", Journal of Applied Mechanics, Vol 31, Number 7, July 1960

[7] Low Temperature Thermal and Electrical Conductivities of Normal and Neutron Irradiated Graphite, North American Aviation Report NAA-SR-862, 1 June 1954.

[8] Touloukian, Y. S., Recommended Values of the Thermophysical Properties of Eight Alloys, Major Constituents and Their Oxides, Thermophysical Properties Research Center, Purdue University, February 1966.

The remainder of the network is identical to the coarse network. The radiation resistors included reflected as well as direct diffuse radiation. Emissivity values as recommended by Touloukian were varied as a function of temperature in computing the grey-body shape-factors.

4. Graphite Models

Two analytical models were used in the analysis of the graphite specimen. One model assumed perfect contact between the composite shield composed of a 0.0535-in. P-03 graphite shell, 0.003-in. mica, and a backing plate of 0.02-in.-thick 347 stainless steel. The second model assumed that no contact existed between the graphite shell and backing. The model shown in Figure 2 was used for the case without contact while the perfect contact case used the model shown in Figure 3, with two-dimensional flow in the shell lamina. The backing plate was assumed to be thermally insulated from the heater and heat sink and all heat transmitted through the steel backing plate was assumed to be conducted through the mica. This model had twice as many nodes in the specimen rod and shield shell regions than did the model used for the original uncertainty analysis. An emissivity of 1.0 was assumed for the graphite rod and shell; therefore, all radiation was direct.

Analyses were made for the graphite with thermal conductivities corresponding to values before and after nuclear irradiation. The thermal conductivity versus temperature table was modified for the irradiated specimens to the expected values based upon trend data presented in North American Aviation Report NAA-SR-862.[9]

B. TRANSIENT DRIFT

Transient drift was considered to be a heat leak due to a change of system enthalpy during transient conditions because of the thermal capacitance

[9] op cit., Reference 7.

of the specimen heater, thermocouple clamps and the specimen itself. Drift leakage was computed by summing the product of the specimen heat, mass, and rate of temperature change with time for the specimen heater, thermocouple clamps, and specimen. This relationship can be expressed as:

$$\dot{Q}_{Drift} = \sum\left(C_p M \frac{dT}{dt}\right) = \left(C_p M \frac{dT}{dt}\right)_{Heater} + \sum\left(C_p M \frac{dT}{dt}\right)_{Clamps} + \sum\left(C_p M \frac{dT}{dt}\right)_{Specimen}$$

Where:
- $\dot{Q}_{Drift}$ = Heat leakage due to transient drift
- C_p = Specific heat of material
- M = Mass of element
- T = Temperature
- t = Time

Transient drift calculations differ from those contained in the original uncertainty analysis in that the contribution of the specimen is included in the calculations. The specimen was divided into five isothermal elements for the analysis. The diagram of Figure 4 shows this specimen subdivision and the assumptions that were made. The configurations analyzed were:

Specimen Material	Heater Material	Thermocouple Clamp Material	Specimen Dia., In.
Beryllium	Aluminum 6061	Copper	0.175
Aluminum 7039	Aluminum 6061	Copper	0.175
Inconel 718	Aluminum 6061	Copper	0.625
Titanium 5Al 2.5Sn ELI	Aluminum 6061	Copper	0.625
Graphite P-03	Invar	Invar	0.4..

C. TOTAL HEAT LEAK

The total heat leak from the specimen is the sum of the steady-state and transient terms. Leakage for the various specimens are plotted as functions of percent of specimen heater power on Figures 5 through 11. At lower ΔT holds, leakage is primarily the result of transient drift. At higher ΔT holds, however, leakage is predominantly the result of thermal radiation. Steady-state leakage is defined as the maximum difference between the heat flowing from the specimen heater core and the heat conducted through the specimen between the lower and middle or the middle and upper thermocouples. These curves represent the maximum total of transient and steady-state leakage terms disregarding the direction of flow. Leakage terms were always considered to be additive. The transient drift term can be positive (heat flow away from the specimen) if the equilibrium point is approached from a higher temperature. The converse also holds true; that is, the term can be negative if the equilibrium point is reached from a lower temperature. The steady-state leakage is positive for all metallic specimens, and the maximum leakage occurs at the hot end. In contrast to this, the cold end of the graphite specimen gains more heat than is lost at the hot end. As a result, the error is positive at the hot end and negative at the cold end. Therefore, the results plotted in the figures should be used to indicate the accuracy of the experiment rather than as calibration curves to correct test data.

D. DISCUSSION OF RESULTS

1. Beryllium and Aluminum Specimens

The predicted thermal leakage for the specimens at [illegible] was slightly higher than corresponding values shown in the figures of the original uncertainty analysis. By including the transient drift term contributed by the specimen, the leakage at the lower ΔT holds increases. Similarly, the omission of reflected energy in the steady-state analysis increases the thermal leakage at the higher ΔT holds. The experimental [illegible] of these specimens

is still very good, maximum leakage being approximately 2% of specimen heater power.

2. Inconel and Titanium Specimens

The predicted accuracy is poorest for Inconel and titanium specimens. The relatively high thermal capacitance of these materials causes a large transient drift leakage at the lower ΔT holds. At the higher ΔT holds, thermal radiation causes large leakages. The radiation leakage is the result of the mismatch in the temperature distributions of the specimen rod and shield shell. Although the shield shell is the same material as the specimen rod with identical temperatures at thermocouple TC_3 and the sink end, the temperature distribution for a ΔT of approximately 350°K, as shown in Figure 12, is different from that of the specimen rod. This occurs because as much as 75% of the heat conducted along the shell is by-passed by direct radiation and multiple reflections. Consequently, the temperature distribution in the shell is influenced almost as much by radiation as by conduction. This problem could be minimized either by increasing the thickness of the shell from 0.020-in. to 3/16-in., plating the shell with gold or silver to reduce the surface emissivity, or both. A titanium specimen with a 0.020-in.-thick shell was analyzed with a surface emissivity of 0.025 representing a gold or silver plate. This analysis showed that, for a ΔT of 350°K, the maximum heat leak is 3% of the heater power. This represents a 91.5% improvement over the actual setup.

3. Graphite Specimen

The thermal leakage curves published in the original uncertainty analysis, Report RN-S-0424, indicated higher leakages than those indicated in this analysis. The reason for this difference is twofold. First, the original analysis was made with the coarse network. Second, intimate contact was assumed between the graphite shell, mica filler and an aluminum backing plate. Actually, the .003-in.-thick mica filler affords little thermal

resistance, while the 0.05-in.-thick aluminum backing plate provides a better heat transfer path than the graphite shell by approximately 8 to 1. Therefore, the leakage of heat to the backing plate greatly influences the temperature distribution in the shell. Figure 13, which is a temperature plot for a specimen ΔT of approximately 350°K, shows this effect. The significant difference in temperature between the specimen rod and shell, together with an assumed emissivity of 1.0, result in large thermal leakages. To reduce the leakage, a backing plate of 0.02-in. stainless steel was recommended. The thermal resistance of the 0.02-in.-thick steel backing plate is approximately 25 times greater than the 0.05-in.-thick aluminum shell. Figures 8 and 10 illustrate the results for the case in which intimate contact with the steel backing plate was assumed for liquid nitrogen and Freon 114 baths, respectively. Approximately 90% of the reduction in heat leakage from the predictions of the original analysis results from the improved backing plate. The remaining 10% stems from use of the finer network. Figure 14 shows the temperature distribution in specimen rod and shell with steel backing for a specimen ΔT of 350°K. Although the temperature difference between the rod and shell is less than that shown in Figure 13, it still is considerable. The assumption that the shell and backing plate are in intimate contact is conservative. A less conservative estimate would be that 25% of the total shell and backing surfaces are in contact at room temperature. At the boiling temperature of liquid nitrogen, actual surface contact might be increased to 50% due to differential contraction of the steel backing plate and graphite shell. At the maximum specimen ΔT of 350°K, the contact probably would vary from 50% at the sink end to zero at the hot end. Therefore, the assumption that the surfaces of the shell and backing are not in contact is more realistic.

Several other runs of irradiated graphite specimens were made to investigate the effect of other shell materials on thermal leakage. These analyses were made assuming a homogeneous shell material without composite of shell and backing plate. The materials considered and the results of the analysis are listed in the following table.

EFFECT OF SHIELD MATERIAL ON GRAPHITE SPECIMEN ACCURACY

Shield Material	Shield Thickness, in.	Shield Emissivity	Percent Leakage at $\Delta T = 350°K$
Aluminum 7039	0.05	f(T)	25
CRES 347	0.02	f(T)	20
CRES 347	0.02	1.0	15
Glass-fiber	---	1.0	27
Graphite P-03	0.0535	1.0	6.5

Results of this analysis indicated that all cases produced poorer results than the graphite shell alone as illustrated on Figure 7. This was due to the significant difference between the temperature distributions in the specimen and shield as seen in Figures 15 through 18. Interestingly, the stainless steel shell with surface emissivity of 1.0 produced better results than the natural surface. The increased direct radiation from the rod and shell itself produced a temperature distribution for the shell that was similar to the specimen rod.

The glass-fiber shell[10]* showed the poorest results because its temperature distribution was a function only of the radiant interchange. Axial conduction was negligible and the insulation assumed a temperature distribution different from that of the specimen rod. The large amount of thermal leakage for the glass-fiber was the result of the assumed emissivity of 1.0 (actual emissivity was probably at least 0.9) together with the assumption of an emissivity value of 1.0 for the graphite and the large temperature difference between rod and shell as seen on Figure 18. The glass-fiber insulation could be used effectively only for applications in which a small axial temperature gradient exists and with specimens of low emissivity.

[10] *Glass-fiber was assumed to be wrapped around the specimen with a space provided for cooling gas flow around the specimen during irradiation.

E. REFERENCE TEMPERATURE UNCERTAINTY

The reference ring temperature bias term depends upon the temperature rise of the reference ring above the boiling temperature of the reference bath. Because the reference ring is not in the direct path of heat transfer from the specimen and shield, there is assumed to be no temperature gradient between the reference ring and surface in contact with the reference bath. Therefore the temperature bias is assumed to be equal to the temperature differential across the boiling film between the reference bath and copper cap of the test cell.

The calculations made for liquid nitrogen bath and presented in the original uncertainty analysis have been extended to include Freon 114 as a reference bath for all specimens. These calculations are plotted on Figures 19 through 22. The temperature differential across a boiling Freon 114 film is considerably greater than that for liquid nitrogen and results in a reference temperature bias approximately six times as large. The data obtained from ASHRAE Handbook of Fundamentals[11] and used for computing the temperature differential across a pool-boiling film did not cover the entire range of interest; consequently, it had to be extrapolated.

F. TEMPERATURE MEASUREMENT ERROR

Temperature measurement errors are caused by thermocouple readings of other than the desired specimen temperature. The thermcouple junction is located between the specimen, whose temperature is to be measured, and the shield to which the thermocouple leads are tempered. In other words, the thermocouple leads are connected thermally but not electrically to the shield. Errors are introduced whenever the shield temperature at the tempering point

---

[11] op cit., reference 4.

differs from the specimen temperature at the thermocouple clamp. The magnitude of error is proportional to the ratio of the thermal resistance from the specimen to the thermocouple junction divided by the thermal resistance from the specimen to the tempering point on the shield. The thermal resistance from the specimen to the thermocouple junction consists of: R_1, the contact resistance between the specimen and thermocouple clamp; R_2, the resistance across clamp; and R_3, a composite resistance including the contact resistance between the clamp to mica insulator, the resistance across the .005-in. of mica, and contact resistance between mica and thermocouple junction. The thermal resistance from the thermocouple junction to the tempering point on the shield, R_4, consists of a parallel circuit of 5-mil Chromel and Constantan wire 15.7-in. long. This length is composed of 20 turns of 1/4-in. diameter. The temperature error is $\left|T_{Specimen} - T_{Shield}\right| \times \frac{(R_1 + R_2 + R_3)}{(R_1 + R_2 + R_3 + R_4)}$.

The most significant terms of this relationship are R_1, R_3, and R_4. Contact resistances were computed using data of Clousing and Chao[12] and Graff.[13] Contact pressure, hardness, surface roughness, thermal conductivity and material density are parameters involved in the computation. Contact pressures versus operating temperature were estimated for the various material combinations and presented on Figures 23 and 24.

Copper thermocouple clamps are used for all specimens except graphite. The copper clamp could not be used with the graphite specimen because of the large difference in thermal expansion between the two materials. Although the copper clamp could have been preloaded at room temperature to ensure positive contact at the higher temperature, the graphite would have failed in compression at liquid nitrogen temperature. For this reason, Invar was selected as the clamp material for the graphite specimen because of its similar thermal expansion coefficient. The Invar clamp was preloaded at room

---

12 Clousing, A. M. Chao, B. T., "Thermal Contact Resistance in a Vacuum Environment", ASME Paper No. 64-HT-16

13 Graff, W. J., "Thermal Conductivities Across Metal Joints," Machine Design, September 15, 1960, pp, 166

temperature sufficient to cause a deflection of 0.005-in. This preload results in a contact pressure for the Invar-graphite combination of 7500 psi, which remains nearly constant with temperature. It was impossible to estimate the preload on the other specimens because the test cells were sealed before calculations were completed. However, all clamps were installed tightly to ensure good mechanical connections.

The thermal resistance of the 15.7-in. length of thermocouple wire between the junction and shield was found to greatly overshadow all other thermal resistances. The thermal resistance of the circuit between the specimen and junction ($R_1 + R_2 + R_3$) is only 0.4% of the resistance found in the thermcouple tempering leads, R_4. For this reason, only the maximum errors were computed. These errors are presented on Table I.

IV. CONCLUSIONS

Experimental accuracy for the aluminum and beryllium specimens is very good, with a maximum heat leak of approximately 2% of specimen heater power. The leakage for graphite is good up to room temperature with a maximum leakage of about 5% of specimen heater power. This is based on the assumption that the shield and backing are not in contact. The titanium specimen has the poorest accuracy with maximum leakage in excess of 10% of specimen heater power. A supplementary reference bath of Freon 114 could be used to improve experimental accuracy at temperatures above room temperature to about 700°K. However, the large temperature drop across the boiling Freon 114 film causes a large bias in thermocouple reference temperature. This suggests the need for direct temperature measurement at the reference ring.

Temperature measurement error at thermocouples TC_1, TC_2, and TC_3 is negligible because of the predominance of thermocouple wire thermal resistance between the junction and the shield.

TABLE I
TEMPERATURE MEASUREMENT ERROR

Specimen Material	Shield Material	$TC_3 - TC_1$ °K	$T_{Specimen} - T_{Shield}$ At TC_2 °K	Error TC_2 °K	$T_{Specimen} - T_{Shield}$ At TC_1 °K	Error TC_1 °K	NOTE
Beryllium	Beryllium	58	- .370	-.00128	- .707	-.00245	
Beryllium	Beryllium	120	- .842	-.00292	- 1.416	-.00491	
Beryllium	Beryllium	225	- 1.581	-.00549	- 2.350	-.00815	
Aluminum 7039	Aluminum 7039	64	- .065	-.00022	- .194	-.00038	
Aluminum 7039	Aluminum 7039	127	- .234	-.00081	- .344	-.01190	
Aluminum 7039	Aluminum 7039	228	- .931	-.00323	- 1.315	-.00456	
Titanium 5Al-2.5Sn-ELI	Titanium 5Al-2.5Sn-ELI	126	- 4.427	-.0154	- 4.887	-.01696	
Titanium 5Al-2.5Sn-ELI	Titanium 5Al-2.5Sn-ELI	203	-11.556	-.040	-14.863	-.0516	
Titanium 5Al-2.5Sn-ELI	Titanium 5Al-2.5SN-ELI	351	-25.645	-.0990	-61.834	-.2387	
Inconel 718	Inconel 718	136	- 3.250	-.0113	- 3.958	-.01373	
Inconel 718	Inconel 718	204	-11.394	-.0394	-11.790	-.0408	
Inconel 718	Inconel 718	361	-32.469	-.1253	-53.192	-.2053	
Graphite P-03 Unirradiated	Graphite P-03 Unirradiated	119	+ .0097	+.00004	- .00970	-.00004	1
Graphite P-03 Unirradiated	Graphite P-03 Unirradiated	221	+ .0305	+.00012	- .128	-.00052	1
Graphite P-03 Unirradiated	Graphite P-03 Unirradiated	348	- .107	-.00043	- 1.290	-.00521	1
Graphite P-03 Irradiated	Graphite P-03 Irradiated	118	- .281	-.00113	- .690	-.00279	1
Graphite P-03 Irradiated	Praphite P-03 Irradiated	219	- .146	-.00059	- .912	-.00368	1
Graphite P-03 Irradiated	Graphite P-03 Irradiated	323	+ .360	+.00145	- .180	-.00073	1
Graphite P-03 Irradiated	Graphite P-03 Irradiated	215	-12.433	-.0502	-37.264	-.1505	2
Graphite P-03 Irradiated	Graphite P-03 Irradiated	326	+21.632	+.0874	- 6.468	-.0261	2
Graphite P-03 Irradiated	Graphite P-03 Irradiated	77	+ .366	+.00148	+ .330	+.00133	3
Graphite P-03 Irradiated	Graphite P-03 Irradiated	127	+ .684	+.00276	+ .750	+.00303	3
Graphite P-03 Irradiated	Graphite P-03 Irradiated	226	+ 1.126	+.00455	+ 1.267	+.00512	3
Graphite P-03 Irradiated	Graphite P-03 Irradiated	332	+ 1.289	+.00521	+ 1.559	+.00630	3
Graphite P-03 Irradiated	Graphite P-03 Irradiated	124	+ 6.779	+.0274	- 4.833	-.0195	4
Graphite P-03 Irradiated	Graphite P-03 Irradiated	228	+23.696	+.0957	+ 7.490	+.0302	4

NOTES:
1. No contact between graphite shield and backing, liquid nitrogen reference bath.
2. Perfect contact between graphite shield and backing, liquid nitrogen reference bath.
3. No contact between graphite shield and backing, Freon 114 reference bath.
4. Perfect contact between graphite shield and backing, Freon 114, reference bath.

V. RECOMMENDATIONS

A Freon 114 reference bath is recommended for more accurate data above room temperature, provided that an accurate thermocouple is installed at the thermocouple reference ring.

The accuracy for the titanium specimen can be improved at the high ΔT holds by increasing the shield thickness from 0.02 to 3/16-in. Specimen diameter needs to be increased for improved accuracy at low ΔT holds. If the specimen diameter is increased, the length of the specimen as well as the test assembly should also be increased to permit the upper and lower thermocouples to be placed no less than two specimen diameters away from heater or heat sink. This action will ensure one-dimensional flow at the thermocouples. Future tests of titanium specimens should be conducted in a redesigned test cell.

BIBLIOGRAPHY

Uncertainty Analyses for Radiation Effects Tests, Aerojet-General Report RN-S-0424, August 1967.

Thermal Network Analyzer, Aerojet-General Computing Sciences Job 278, 15 August 1962

Boiling Heat Transfer for Oxygen, Nitrogen, Hydrogen, and Helium, NBS Technical Note 317, 20 September 1965.

ASHRAE Handbook of Fundamentals, Chapter 3, P.48, Figure 10

Materials Properties Data Book, Aerojet-General Report 2275, Revised 15 March 1967

Powell, R. L., Hardin, J. L., and Gibson, E. F., "Low-Temperature Transport Properties of Commercial Metals and Alloys, IV. Reactor Grade Be, Mo and W", Journal of Applied Mechanics, Volume 31, Number 7, July 1960

Low Temperature Thermal and Electrical Conductivities of Normal and Neutron Irradiated Graphite, North American Aviation Report NAA-SR-862, 1 June 1954

Touloukian, Y. S., Recommended Values of the Thermophysical Properties of Eight Alloys, Major Constituents and Their Oxides, Thermophysical Properties Research Center, Purdue University, February 1966

Graff, W. J., "Thermal Conductivities across Metal Joints", Machine Design, 15 September 1960, pp. 166-172

Clousing, A. M., Chao, B. T., Thermal Contact Resistance in a Vacuum Environment, ASME Paper No. 64-HT-16

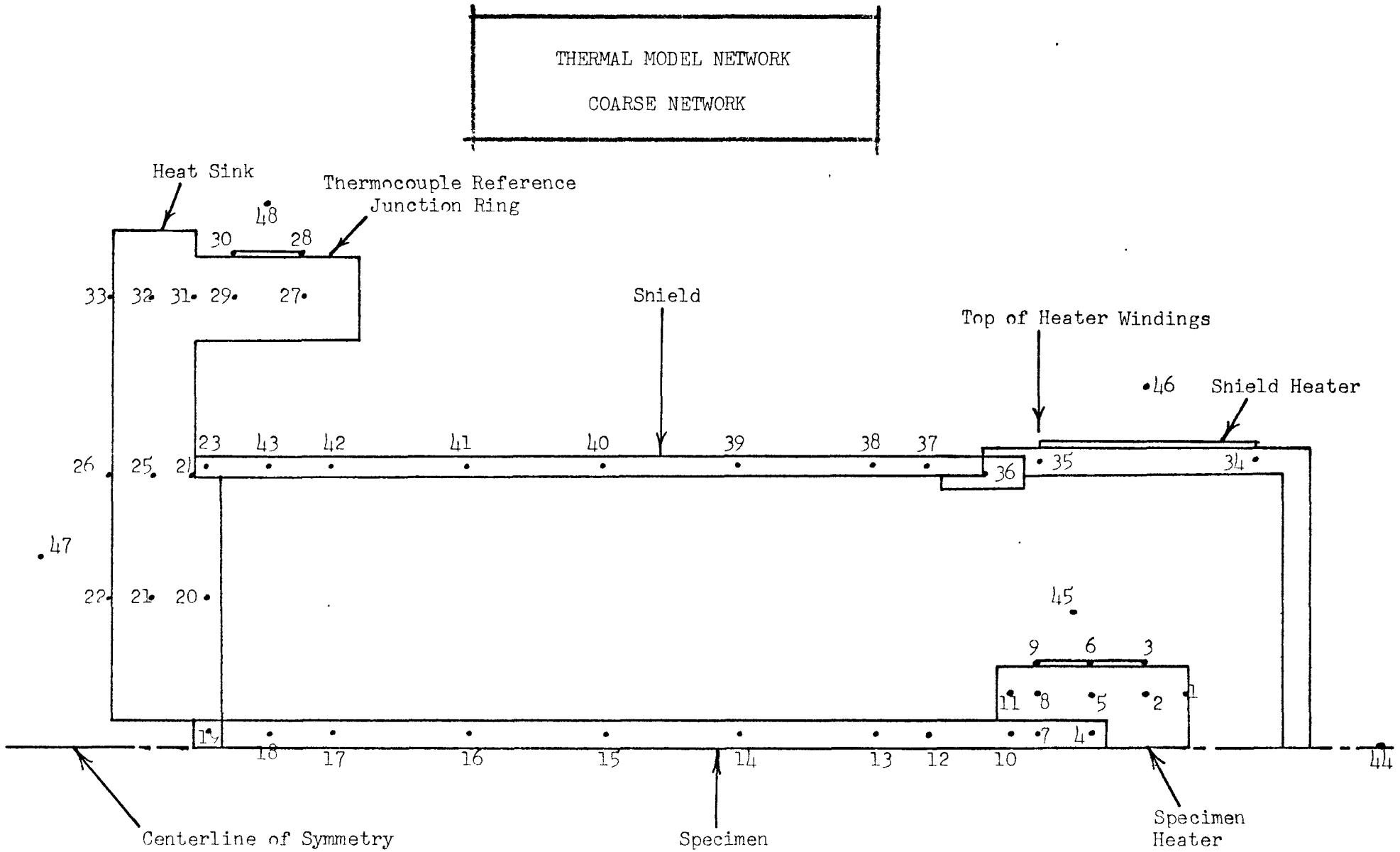
THERMAL MODEL NETWORK
COARSE NETWORK
Heat Sink
Thermocouple Reference Junction Ring
Shield
Top of Heater Windings
Shield Heater
Centerline of Symmetry
Specimen
Specimen Heater
48
30
28
33
32
31
29
27
46
23
43
42
41
40
39
38
37
26
25
24
36
35
34
47
22
21
20
45
9
6
3
11
8
5
2
1
19
18
17
16
15
14
13
12
10
7
4
44

Figure 1

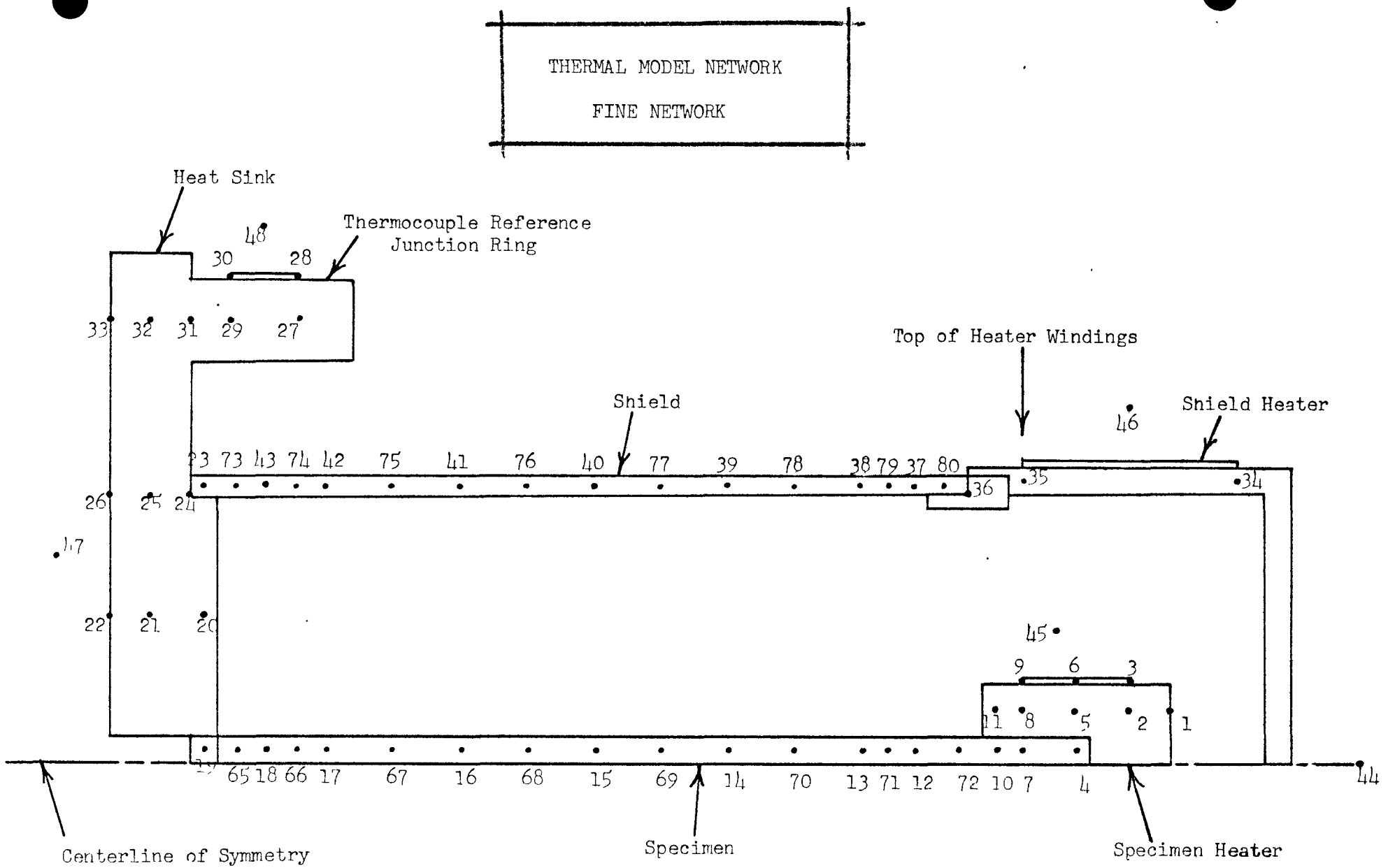
THERMAL MODEL NETWORK
FINE NETWORK
Heat Sink
Thermocouple Reference Junction Ring
Top of Heater Windings
Shield
Shield Heater
Centerline of Symmetry
Specimen
Specimen Heater

Figure 2

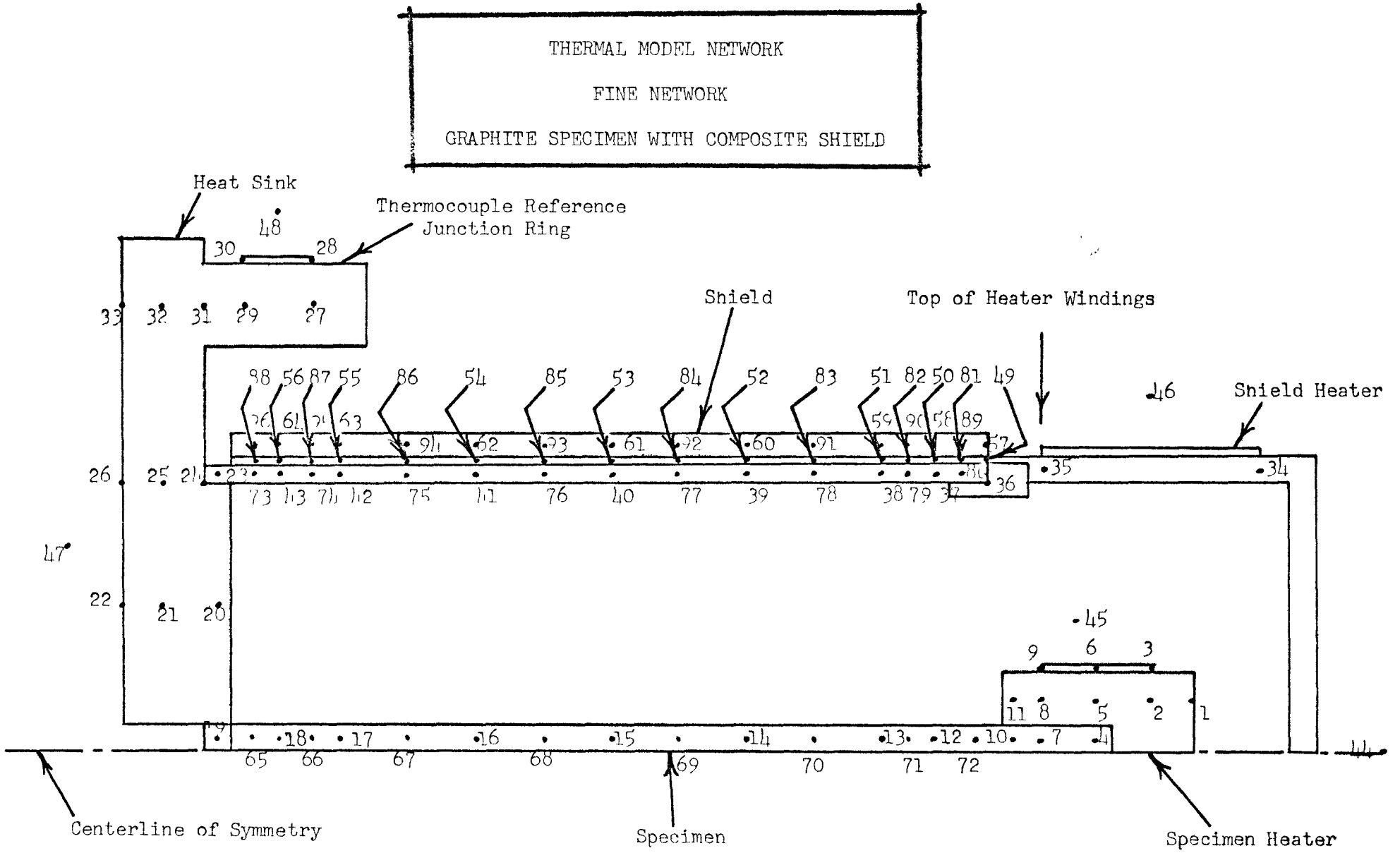
THERMAL MODEL NETWORK
FINE NETWORK
GRAPHITE SPECIMEN WITH COMPOSITE SHIELD
Heat Sink
Thermocouple Reference Junction Ring
Shield
Top of Heater Windings
Shield Heater
Centerline of Symmetry
Specimen
Specimen Heater

Figure 3

TRANSIENT DRIFT DIAGRAM

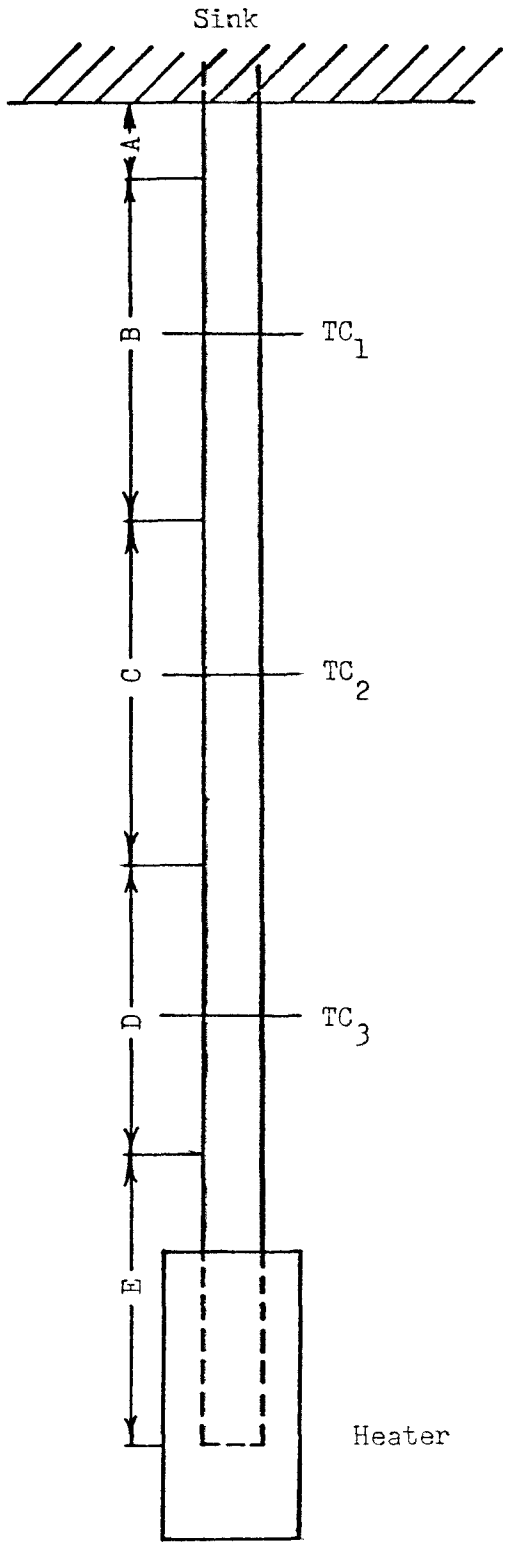

Assumptions:

1. Specimen broken into 5 isothermal elements.
2. Element temperatures:
   $T_A = T_{sink}$
   $T_B = TC_1$
   $T_C = TC_2$
   $T_D = TC_3$
   $T_E = T_{heater}$

Figure 4

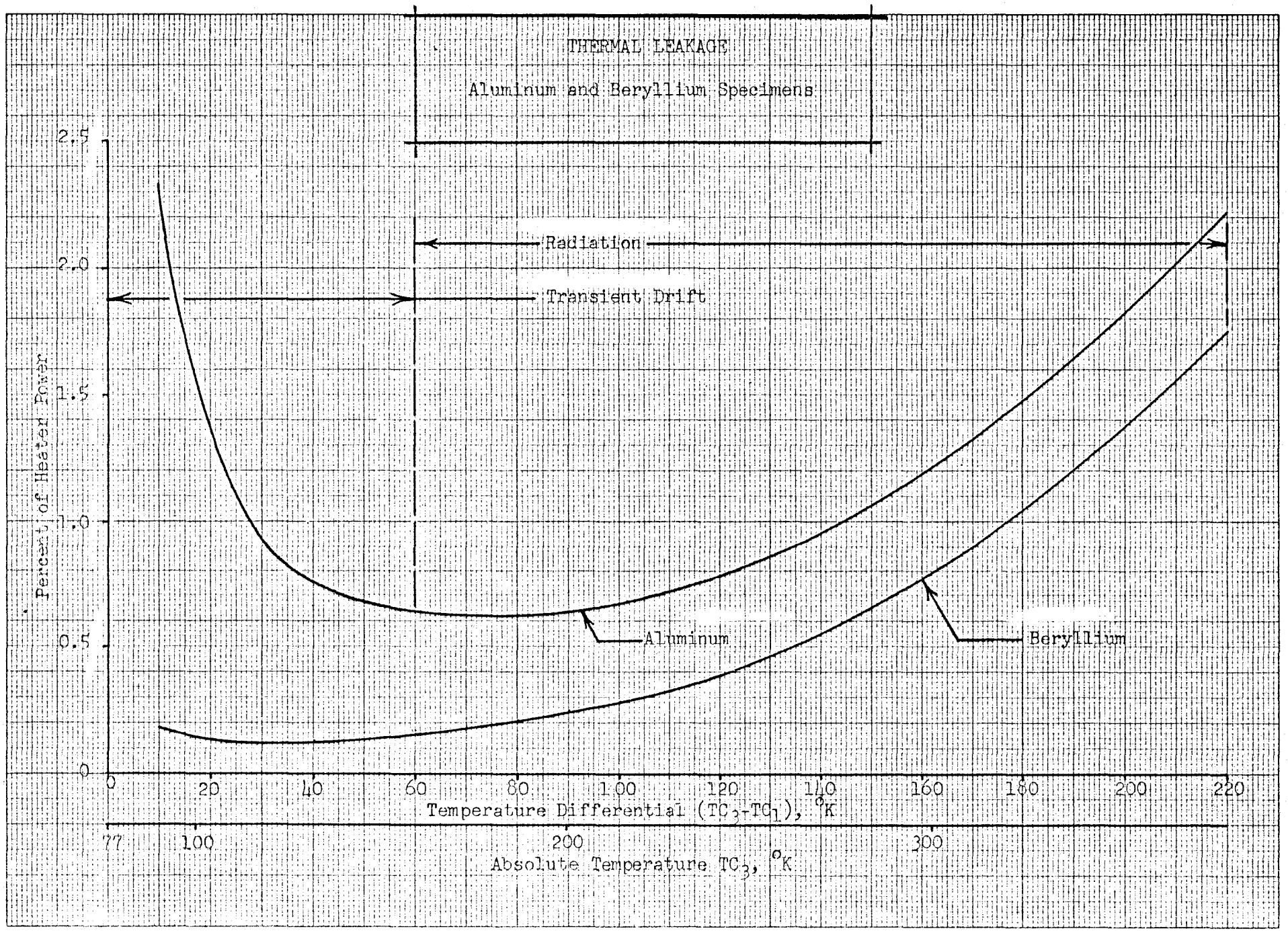

Figure 5

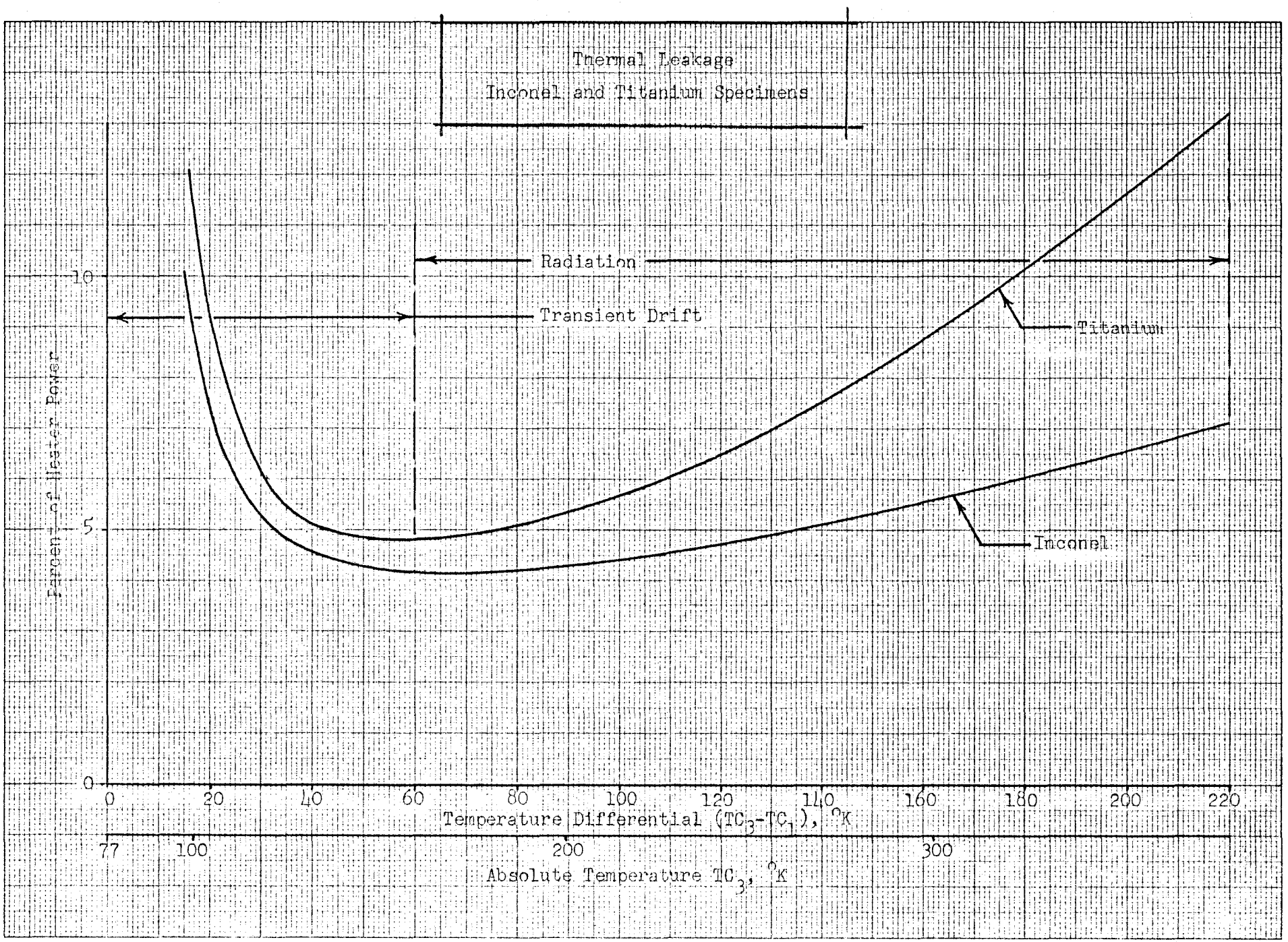

Figure 6

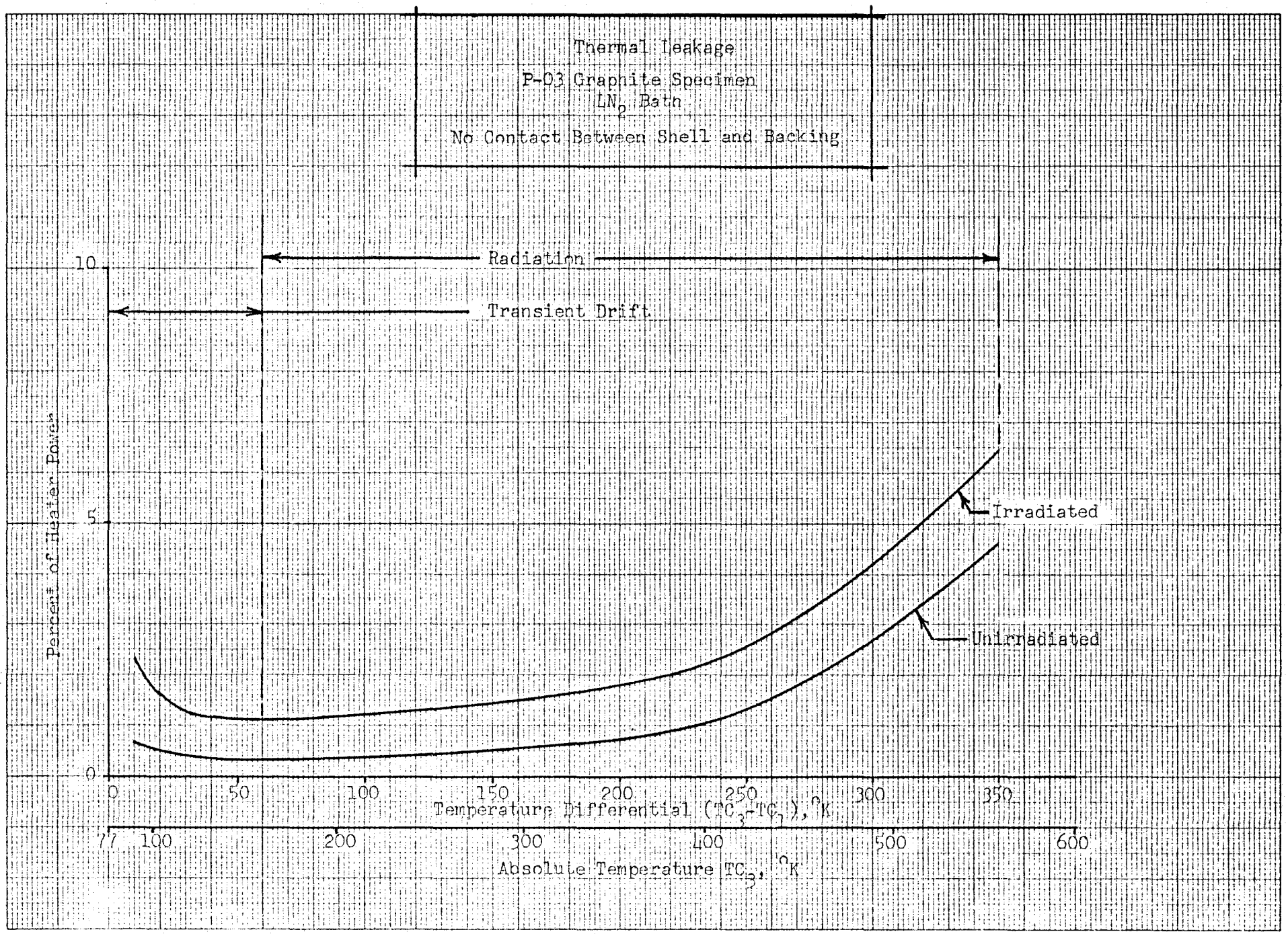

Figure 7

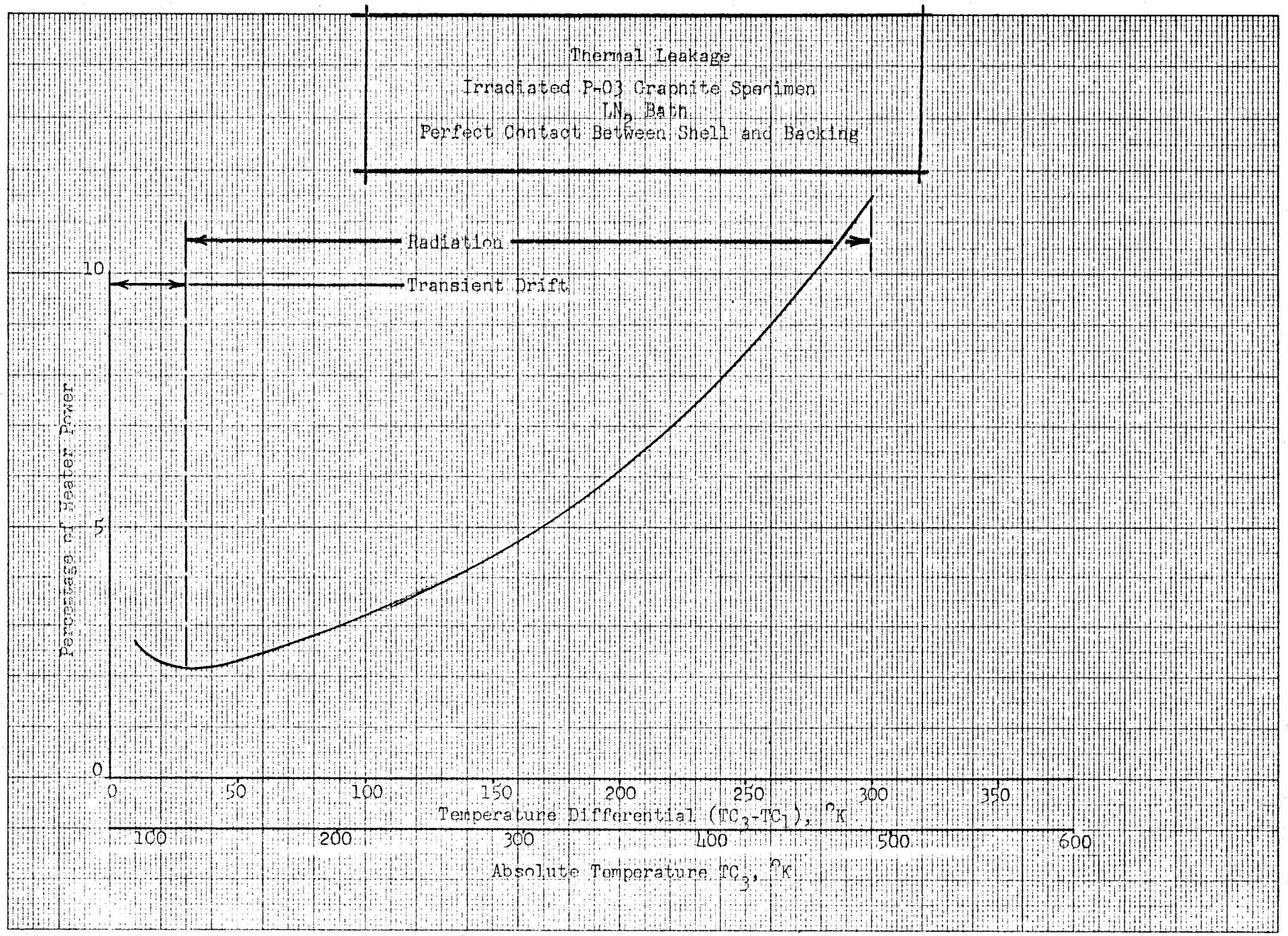

Figure 8

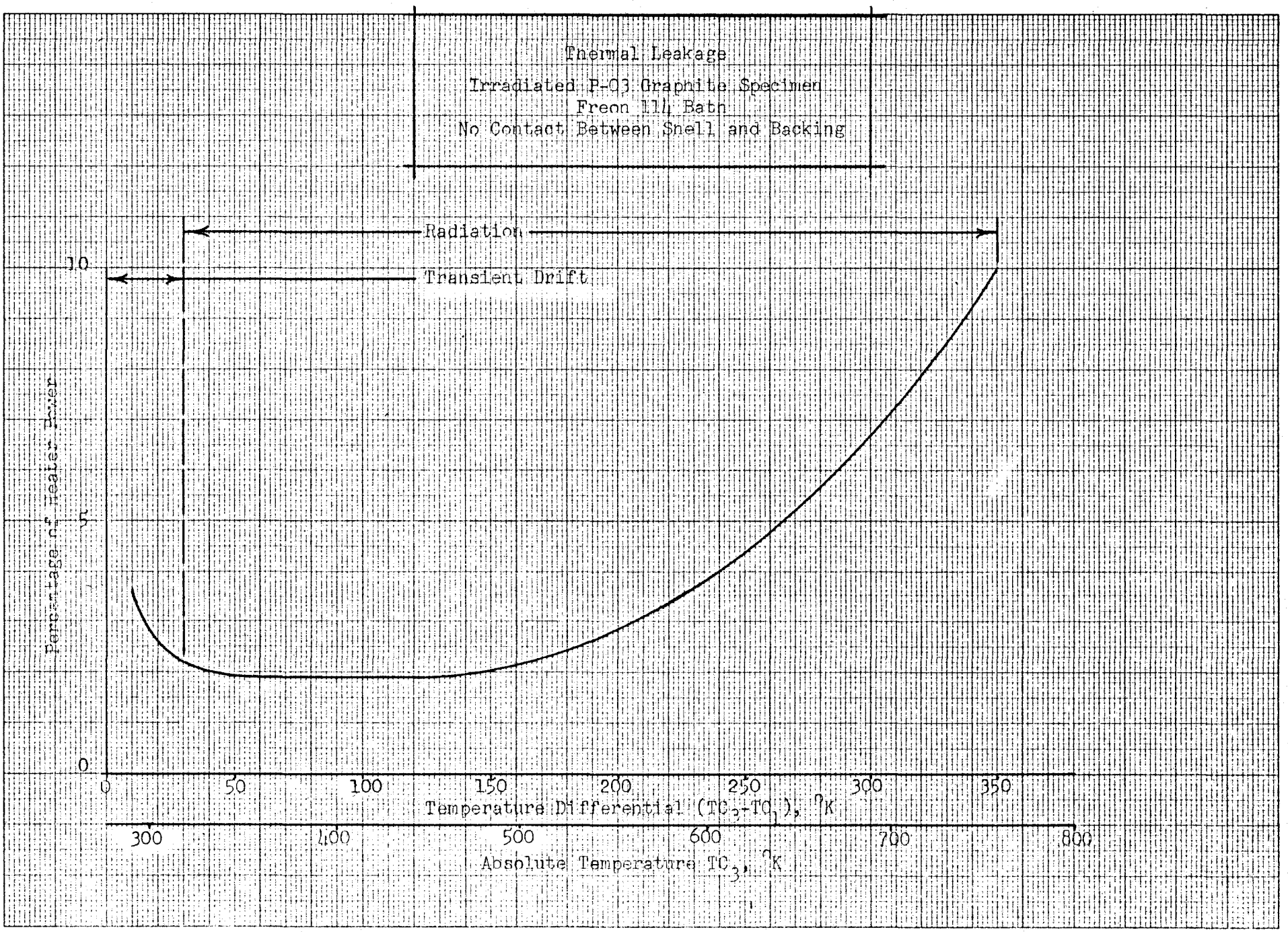

Figure 9

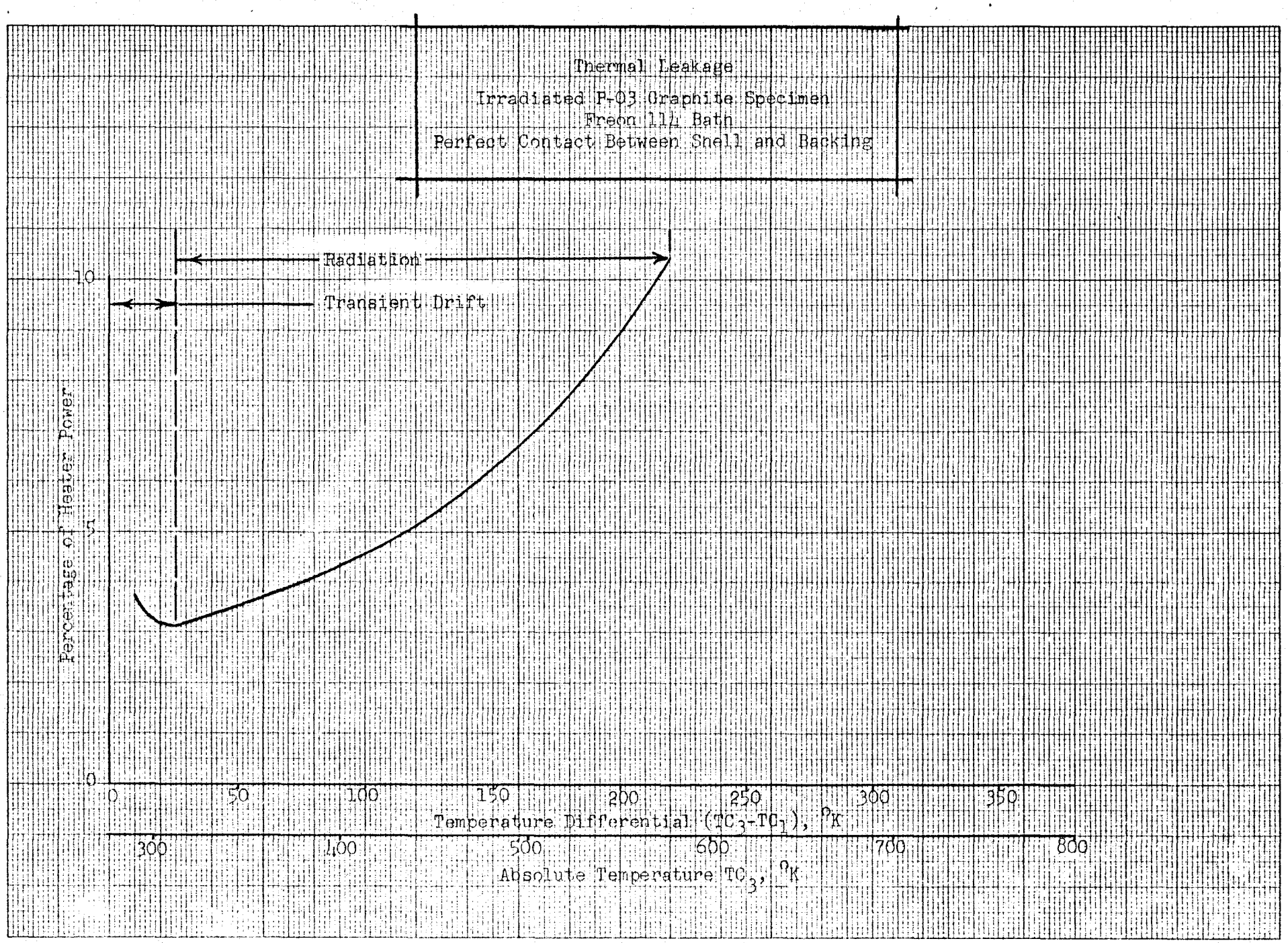

Figure 10

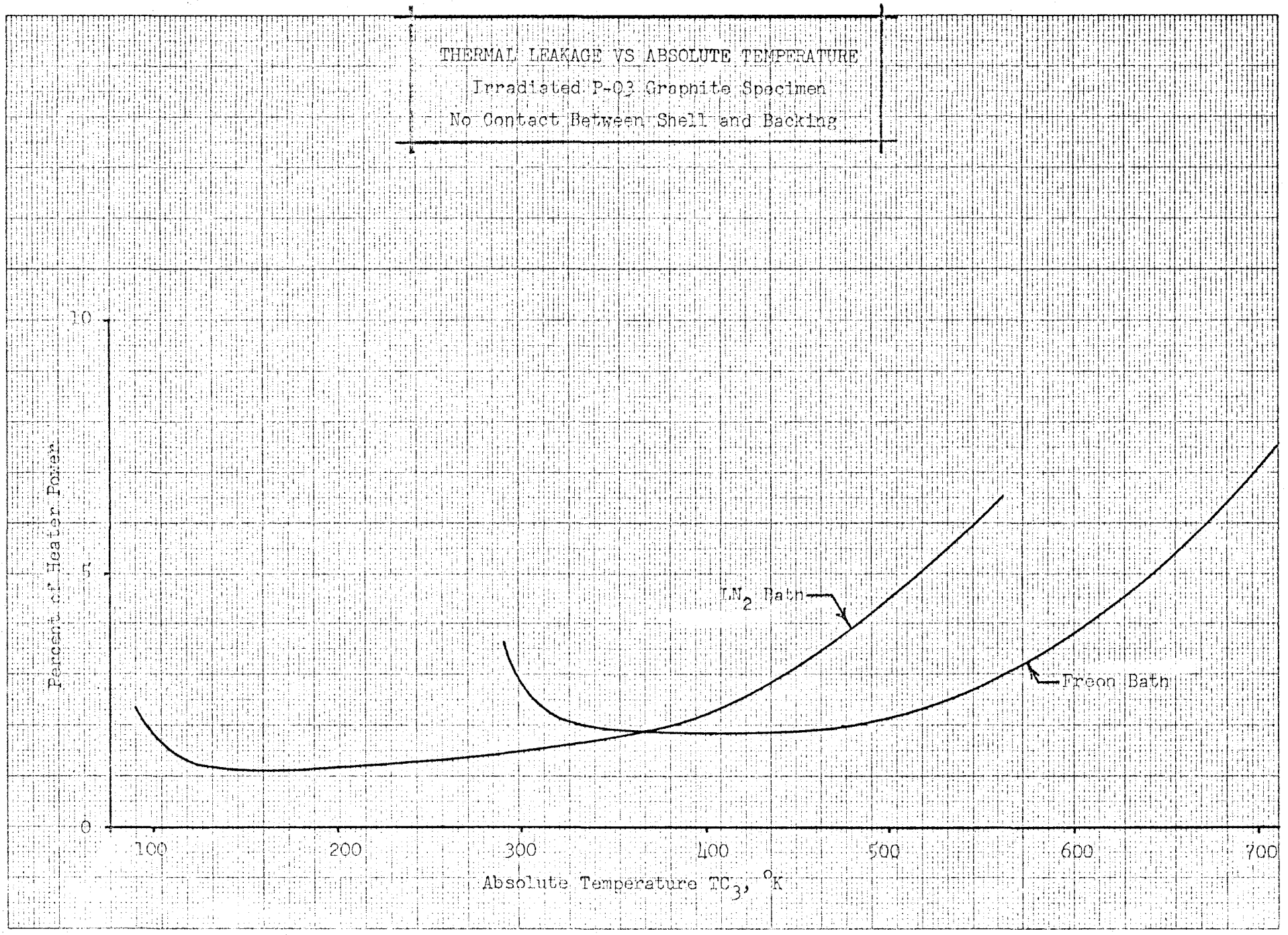

Figure 11

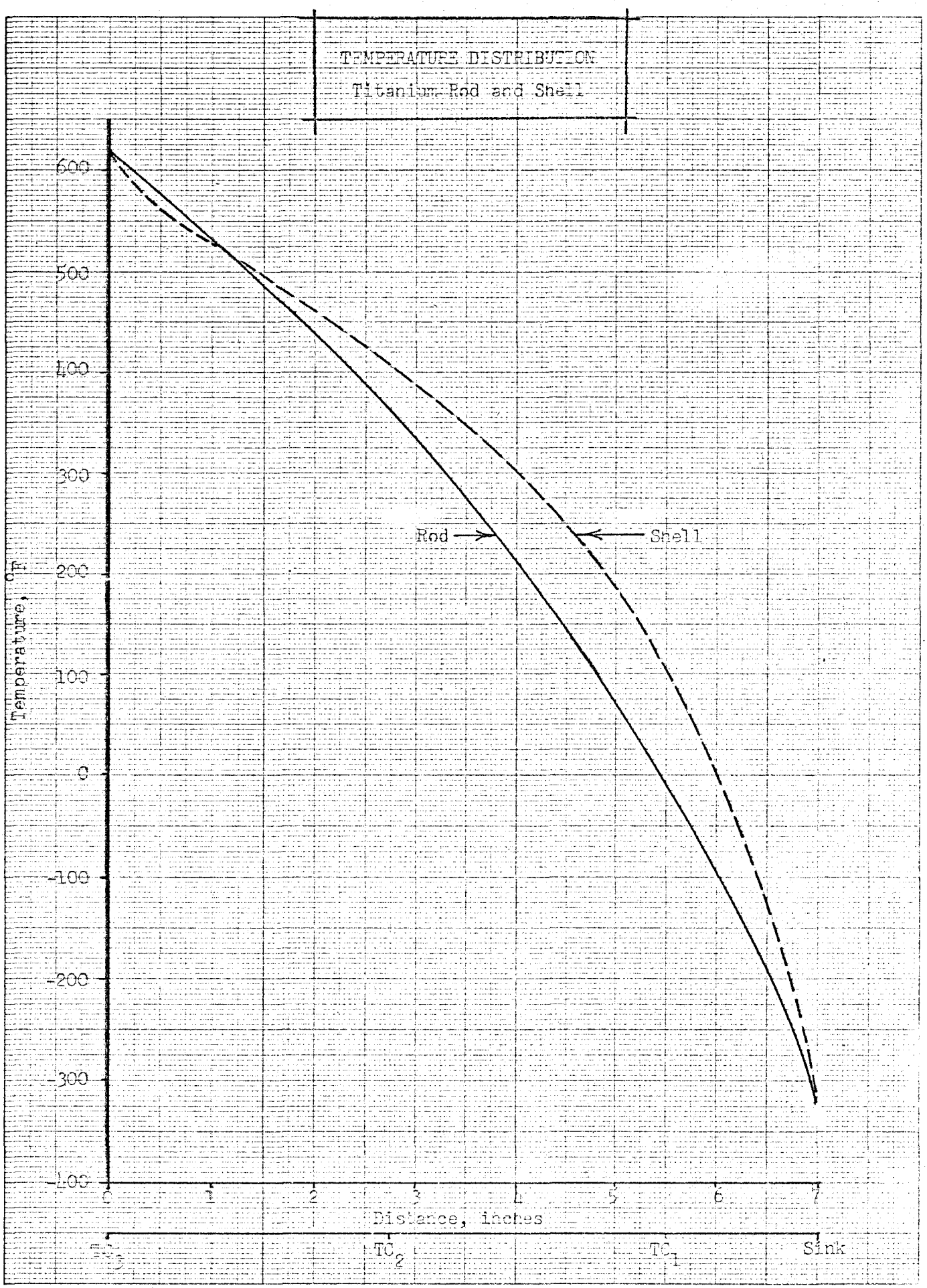

Figure 12

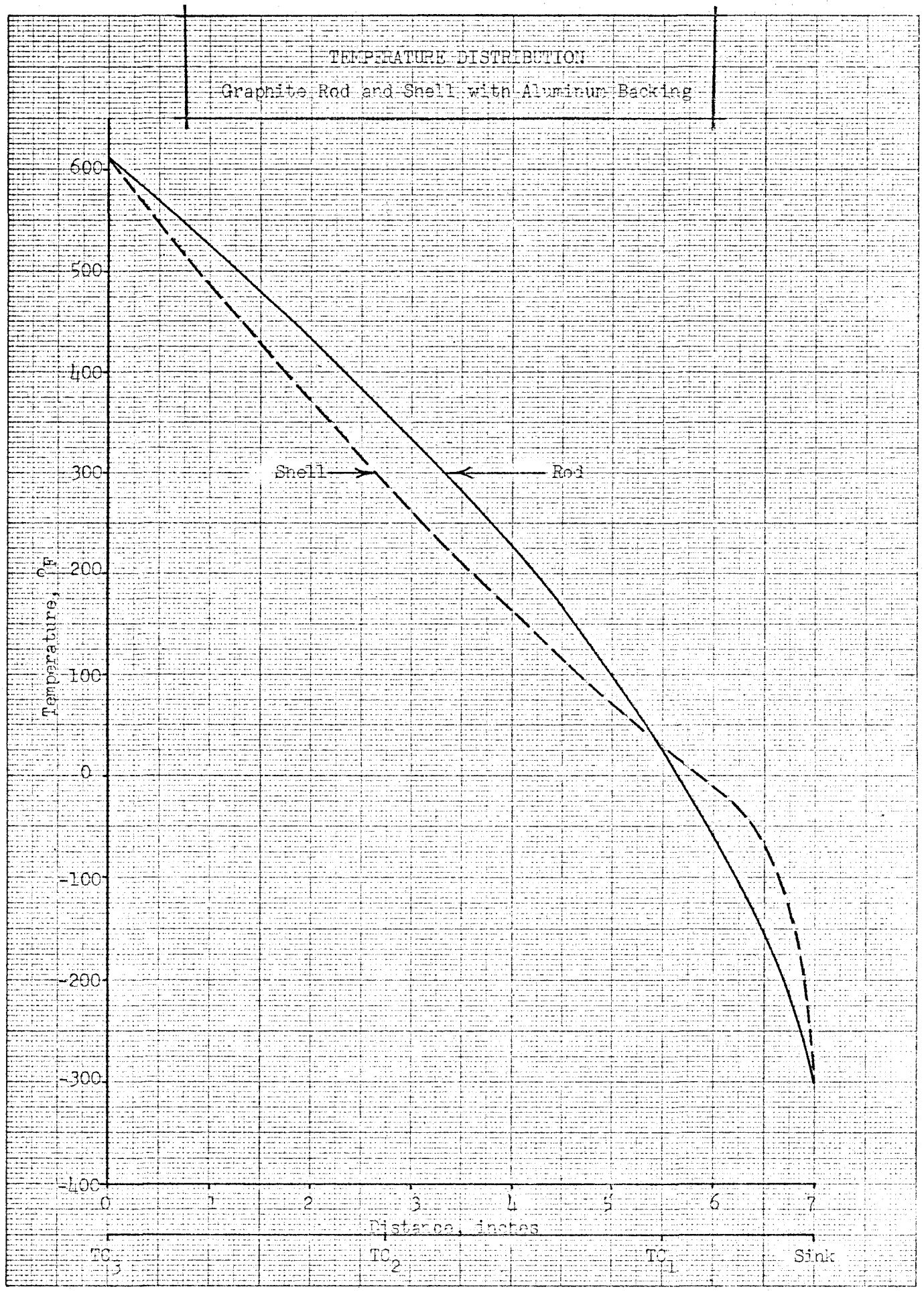

Figure 13

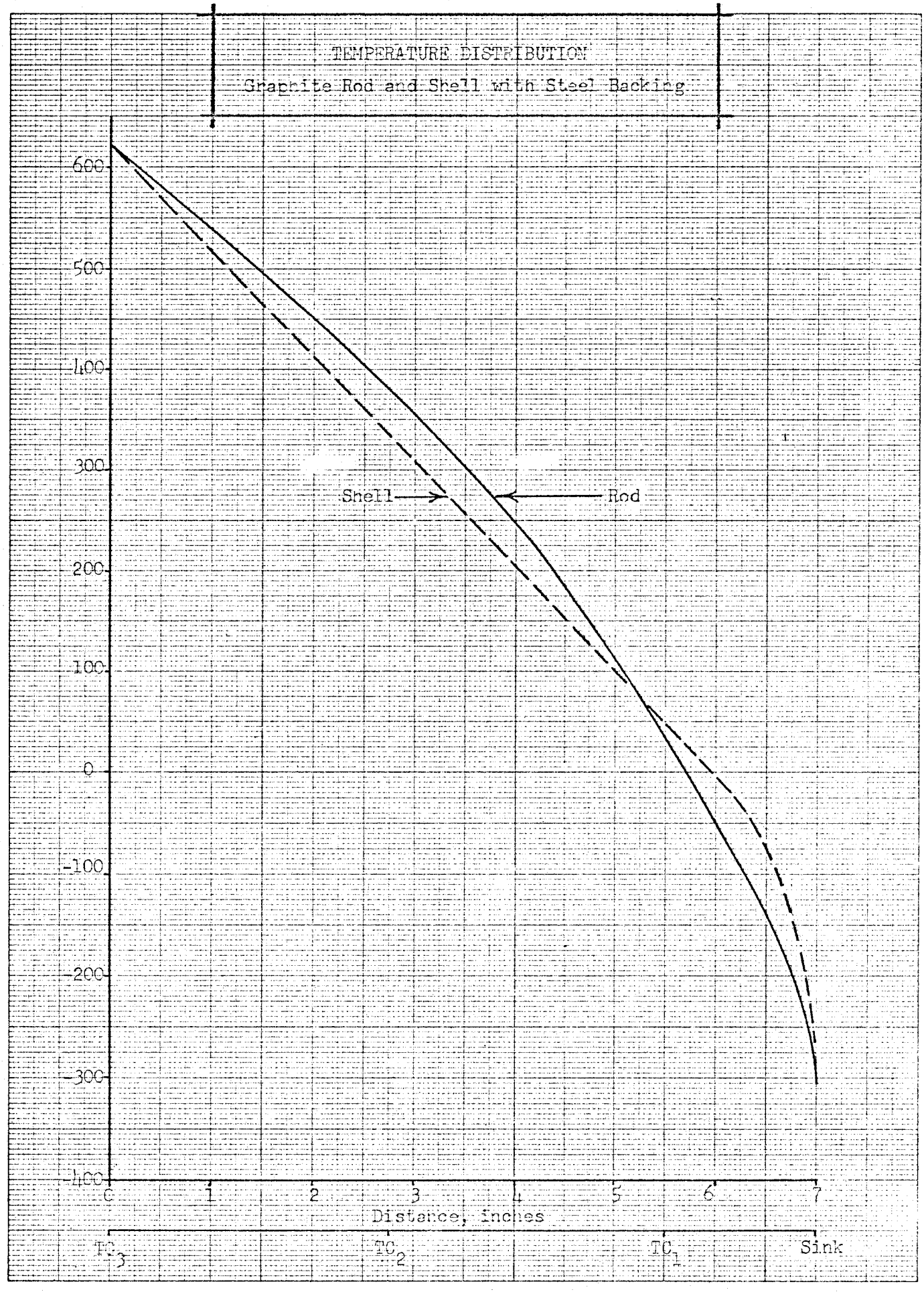

Figure 14

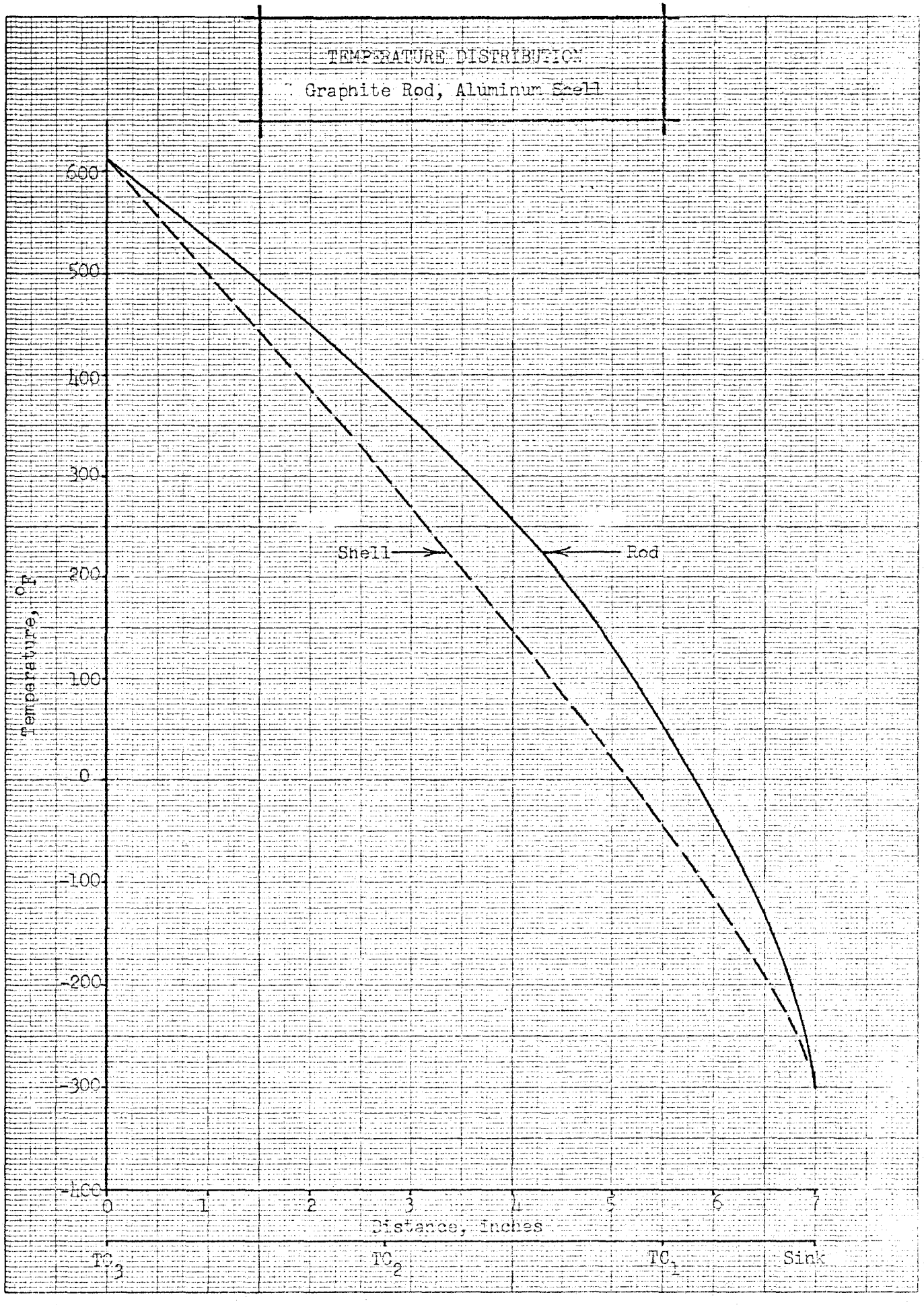

Figure 15

Figure 16

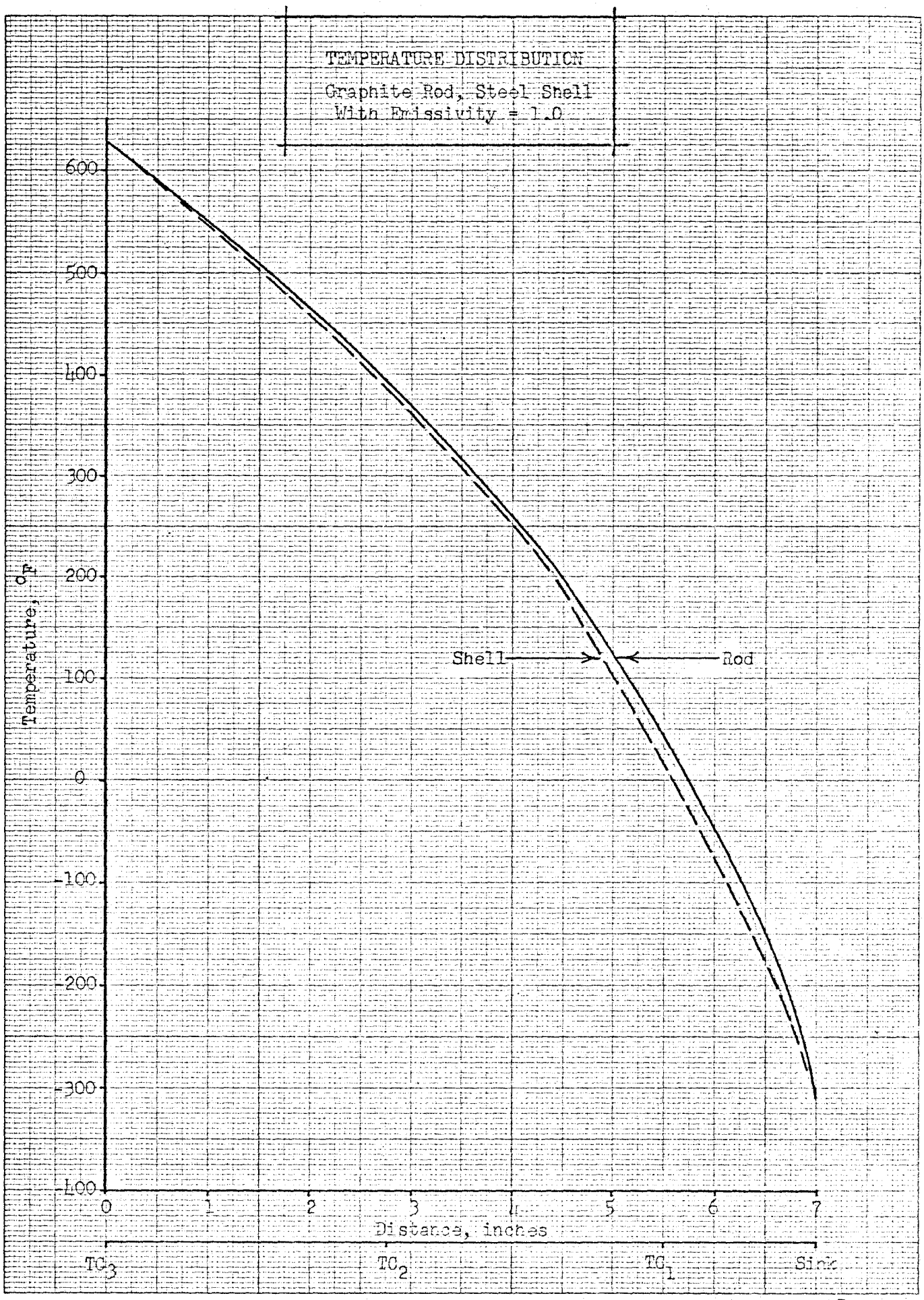

Figure 17

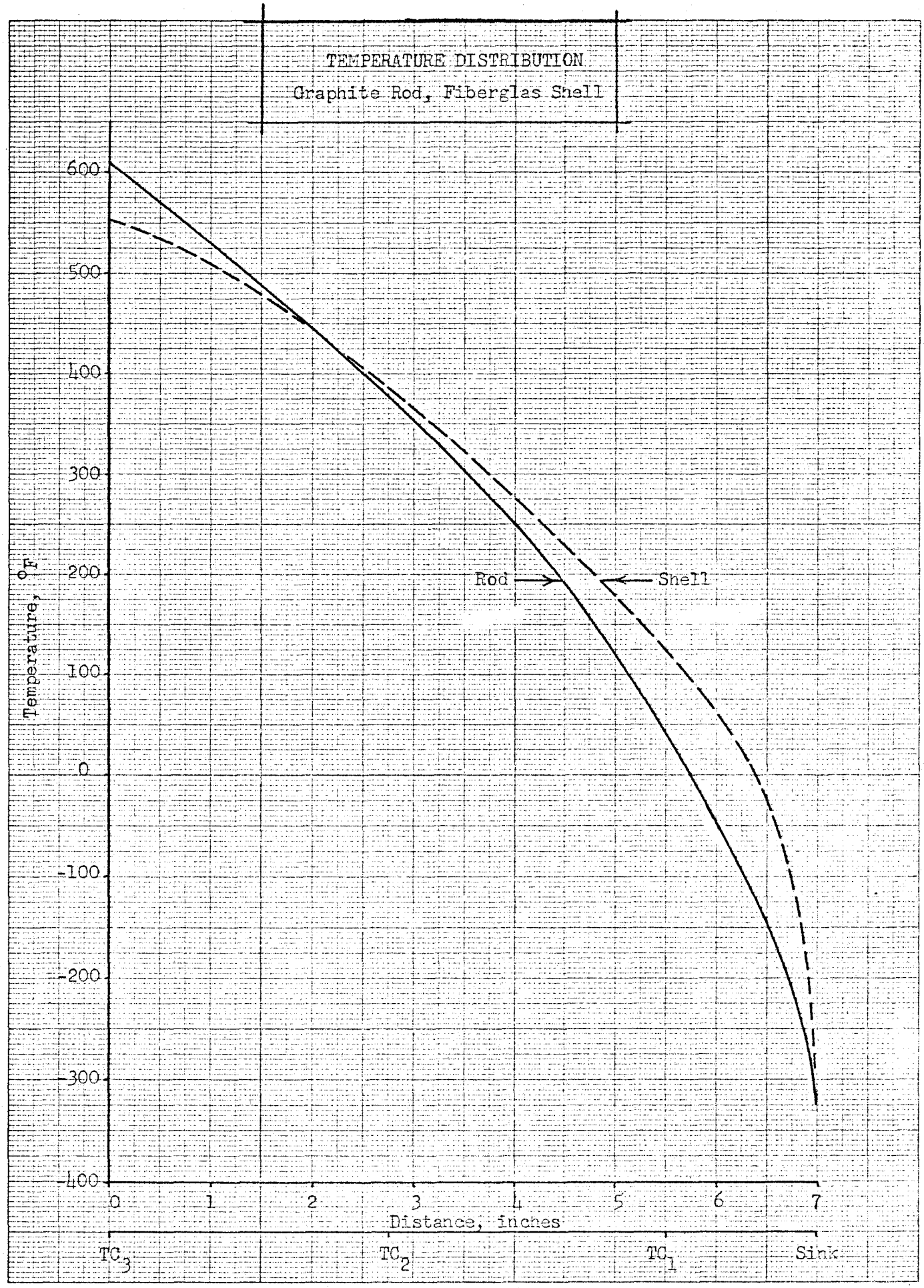

Figure 18

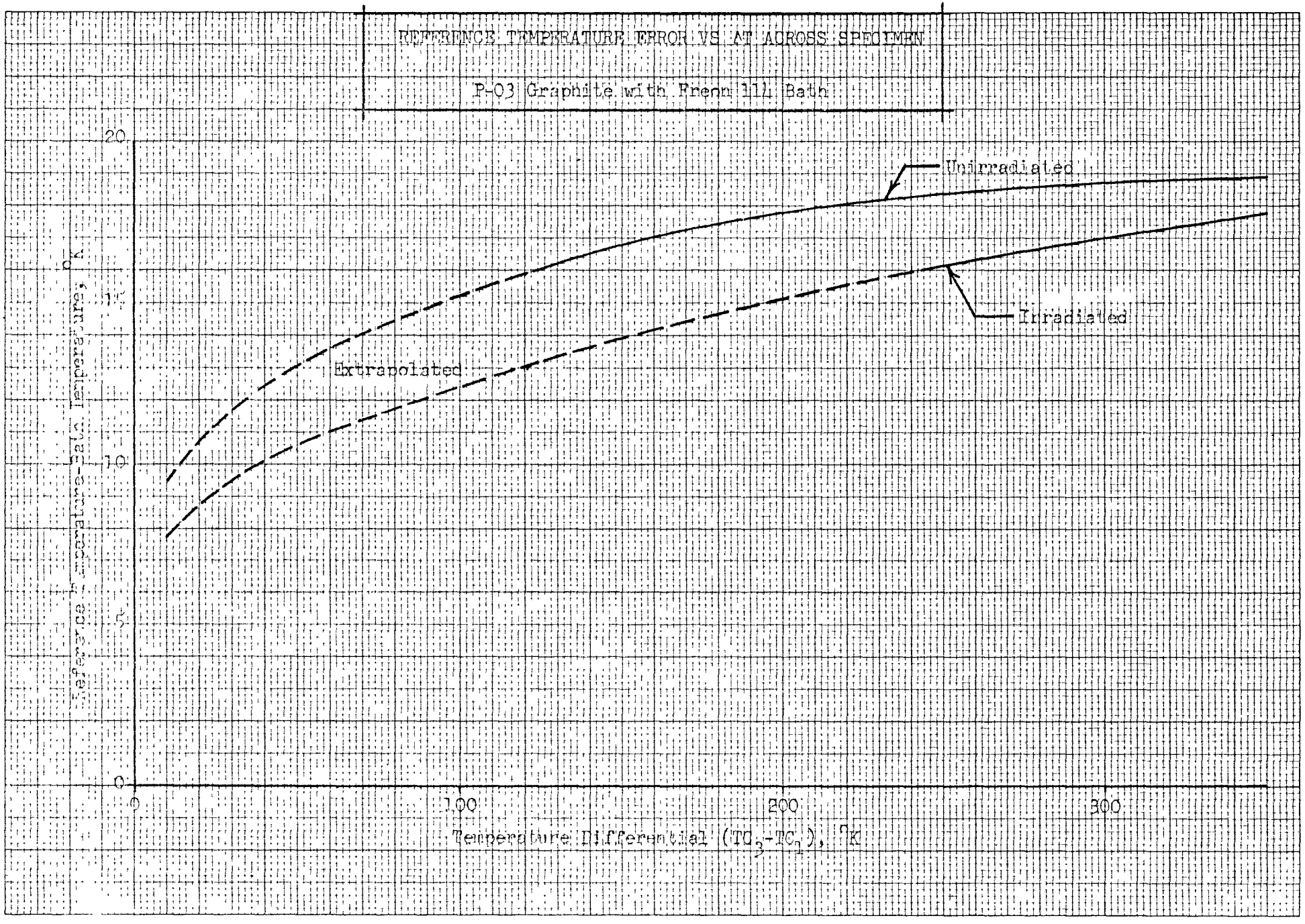

Figure 19

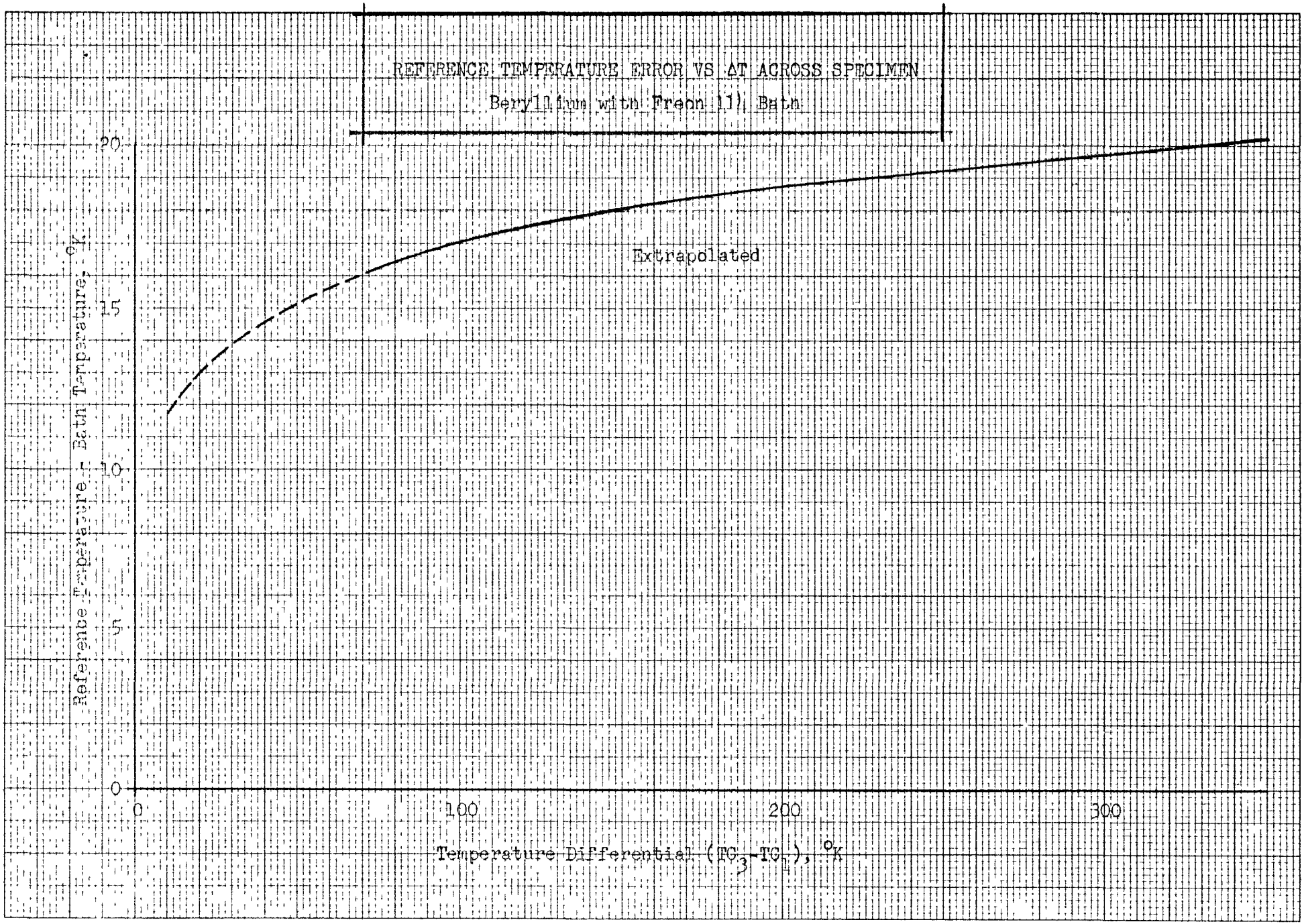

Figure 20

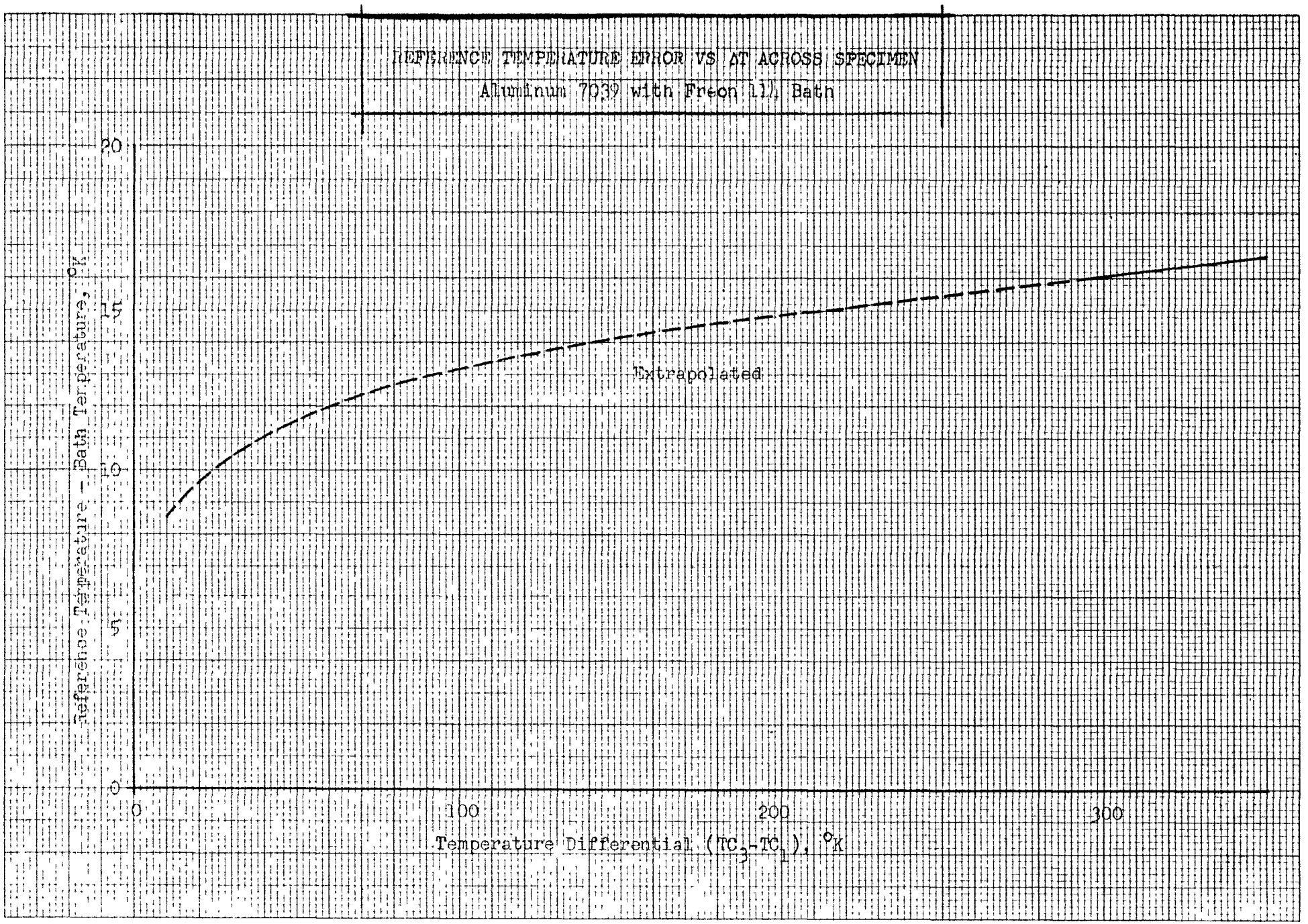

Figure 21

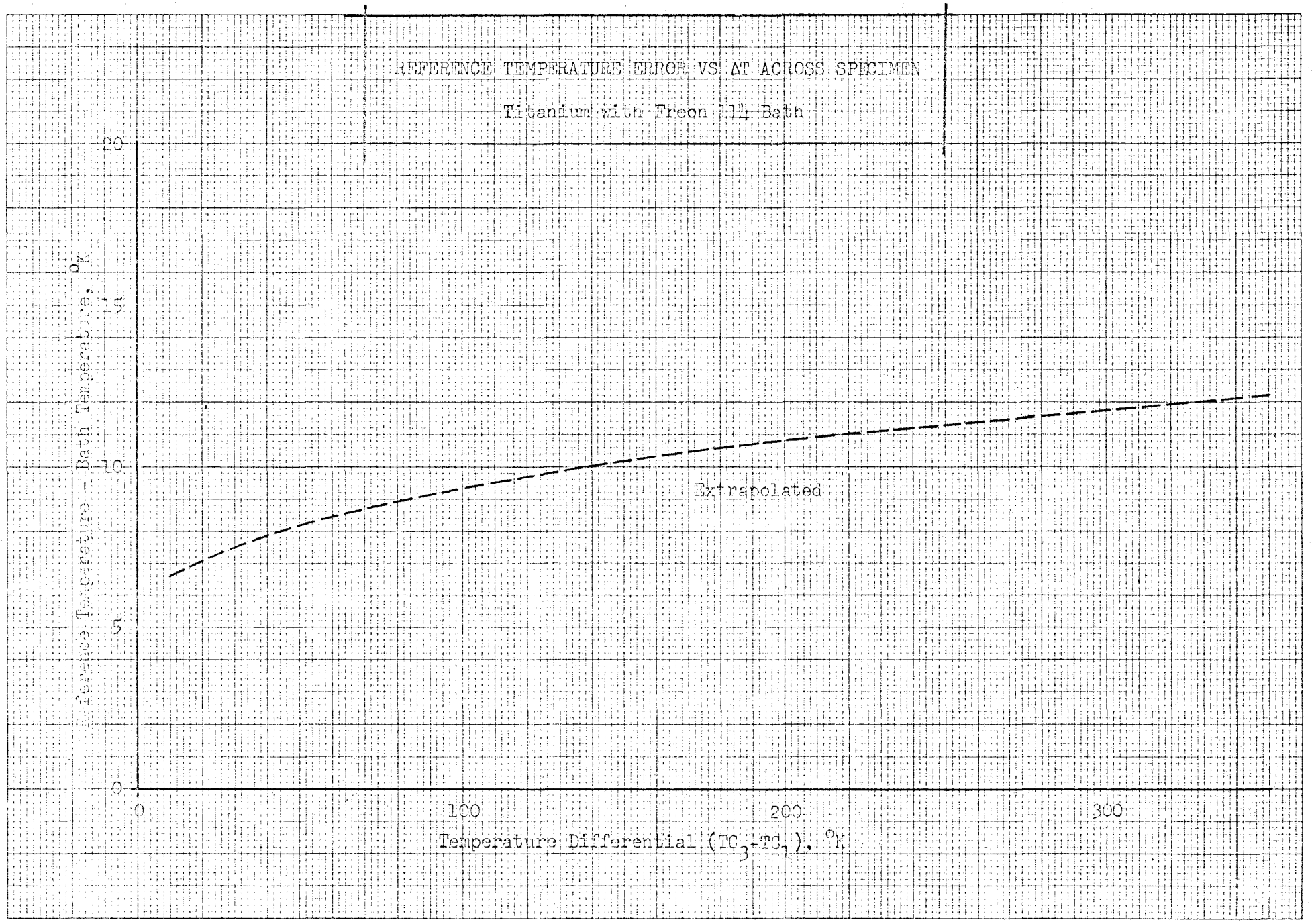

Figure 22

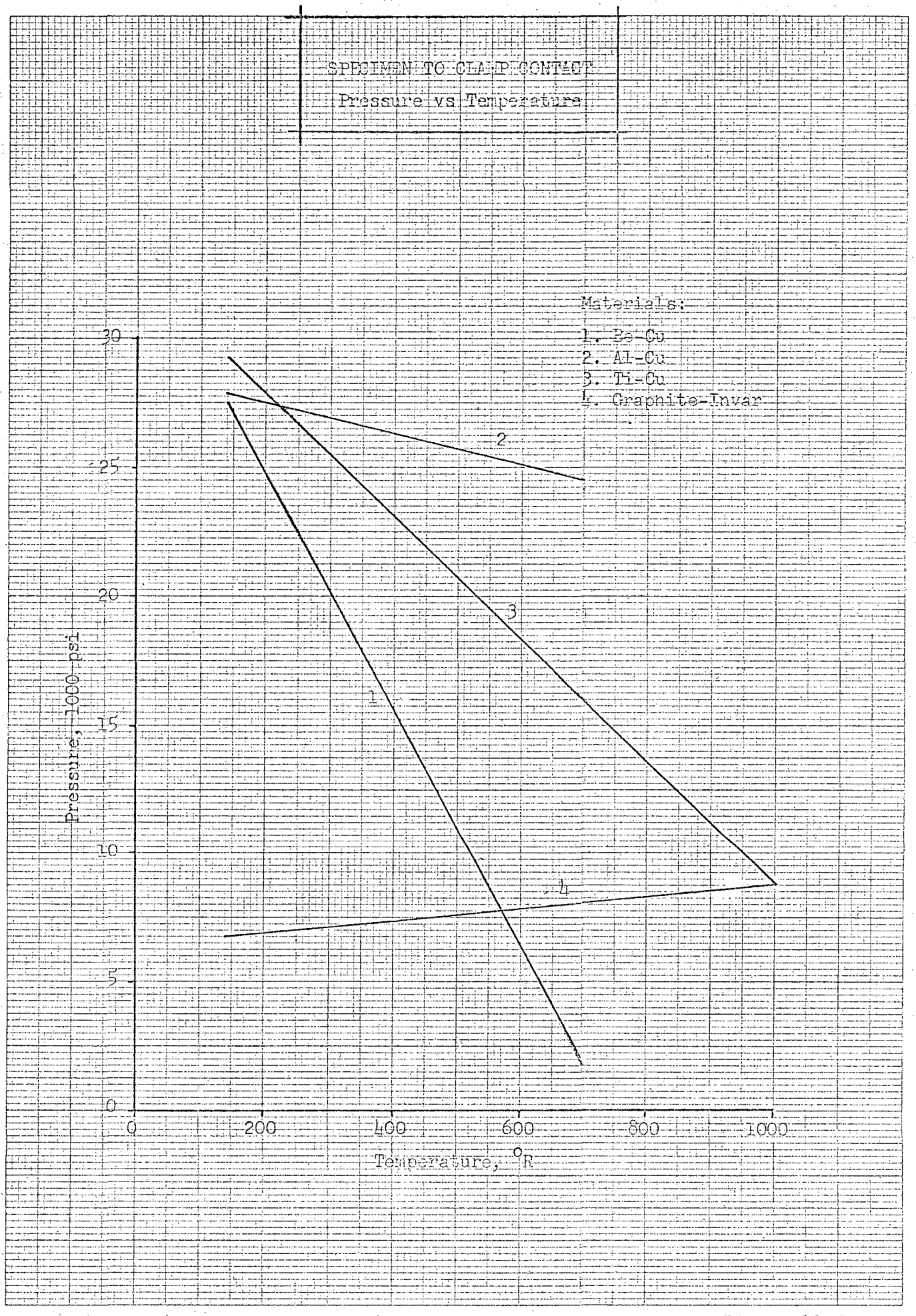

Figure 23

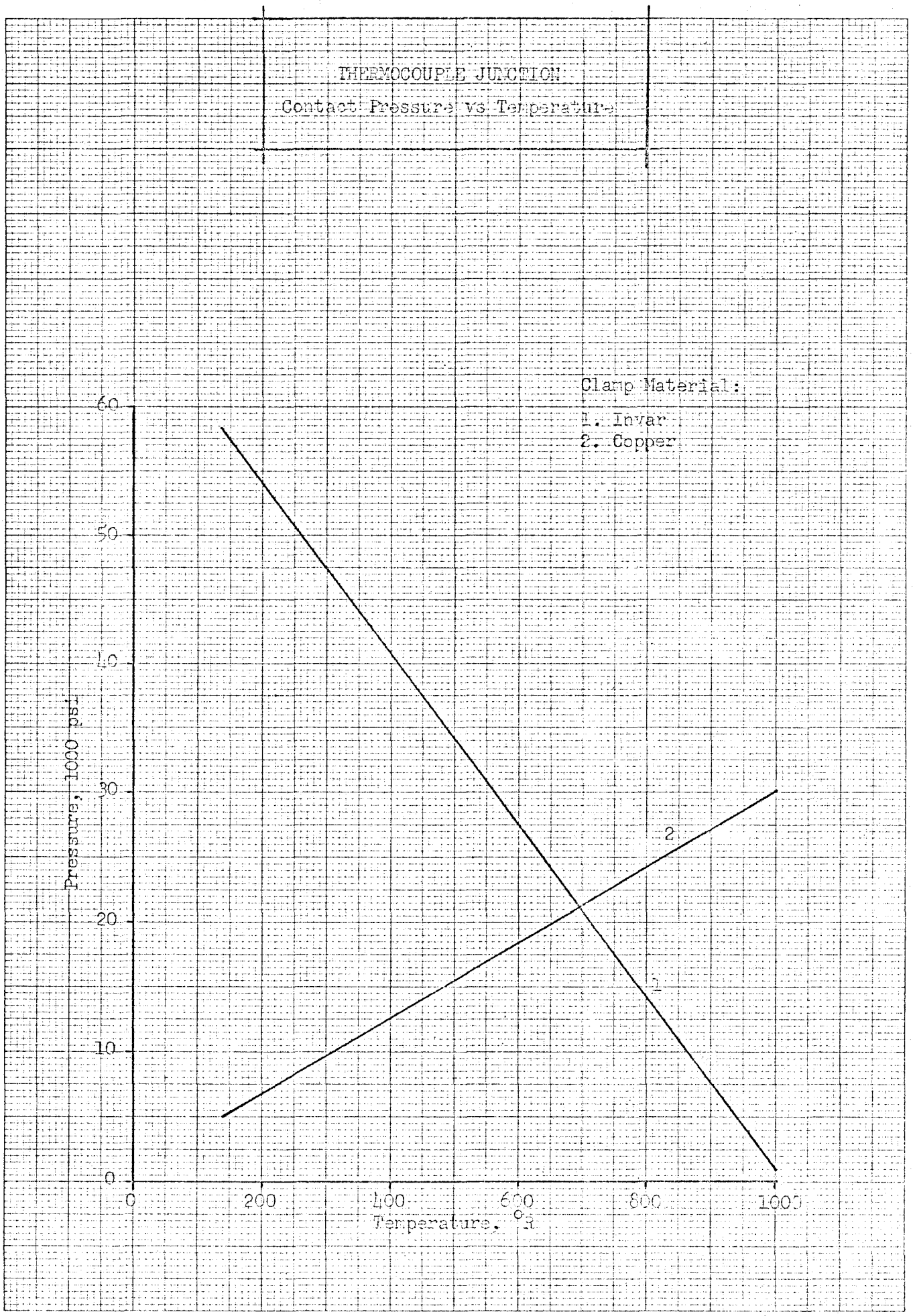

Figure 24